

Two-way feedback mechanism between unfavorable meteorological conditions and cumulative aerosol pollution exists in various haze regions of China

Junting Zhong^{1,2}, Xiaoye Zhang^{1,3*}, Yaqiang Wang¹, Jizhi Wang¹, Xiaojing Shen¹, Hongsheng Zhang⁴, Tijian Wang⁵, Zhouqing Xie^{2,6,7}, Cheng Liu^{2,6,7}, Hengde Zhang⁸, Tianliang Zhao⁹, Junying Sun¹, Shaojia Fan¹⁰, Zhiqiu Gao⁹, Yubin Li⁹, Linlin Wang¹¹

¹Chinese Academy of Meteorological Sciences, China Meteorological Administration, Beijing, 100081, China.

²University of Chinese Academy of Sciences, Beijing 100049, China

³Center for Excellence in Regional Atmospheric Environment, IUE, Chinese Academy of Sciences, Xiamen, 361021, China.

⁴Laboratory for Climate and Ocean-Atmosphere Studies, Department of Atmospheric and Oceanic Sciences, School of Physics, Peking University, Beijing, 100081, China

⁵School of Atmospheric Sciences, Nanjing University, Nanjing, 210023, China

⁶Key Lab of Environmental Optics and Technology, Anhui Institute of Optics and Fine Mechanics, Chinese Academy of Sciences, Hefei, 230031, China

⁷School of Earth and Space Sciences, University of Science and Technology of China, Hefei, 230026, China

⁸National Meteorological Center, China Meteorological Administration, Beijing, 100081, China

⁹Nanjing University of Information Science & Technology, Nanjing, 210044, China

¹⁰Sun Yat-sen University, Guangzhou, 510275, China

¹¹State Key Laboratory of Atmospheric Boundary Layer Physics and Atmospheric Chemistry, Institute of Atmospheric Physics, Chinese Academy of Sciences, Beijing 100029, China

Correspondence to: Xiaoye Zhang (xiaoye@cma.gov.cn)

Abstract. Accompanied by unfavorable meteorological conditions with stable stratification in various haze regions of China, persistent heavy aerosol pollution episodes lasting more than 3 consecutive days (HPEs) frequently occur, particularly in winter. In the North China Plain (NCP), explosive growth in fine particulate matter smaller than 2.5 μm in diameter ($\text{PM}_{2.5}$), which occurs in some HPEs, is dominated by a two-way feedback mechanism between further worsened unfavorable meteorological conditions and cumulative aerosol pollution. However, whether such a two-way feedback mechanism exists in other key haze regions is uncertain; these regions include the Guanzhong Plain (GZP), the Yangtze River Delta (YRD) region, the Two Lakes Basin (TLB), the Pearl River Delta (PRD) region, the Sichuan Basin (SB),

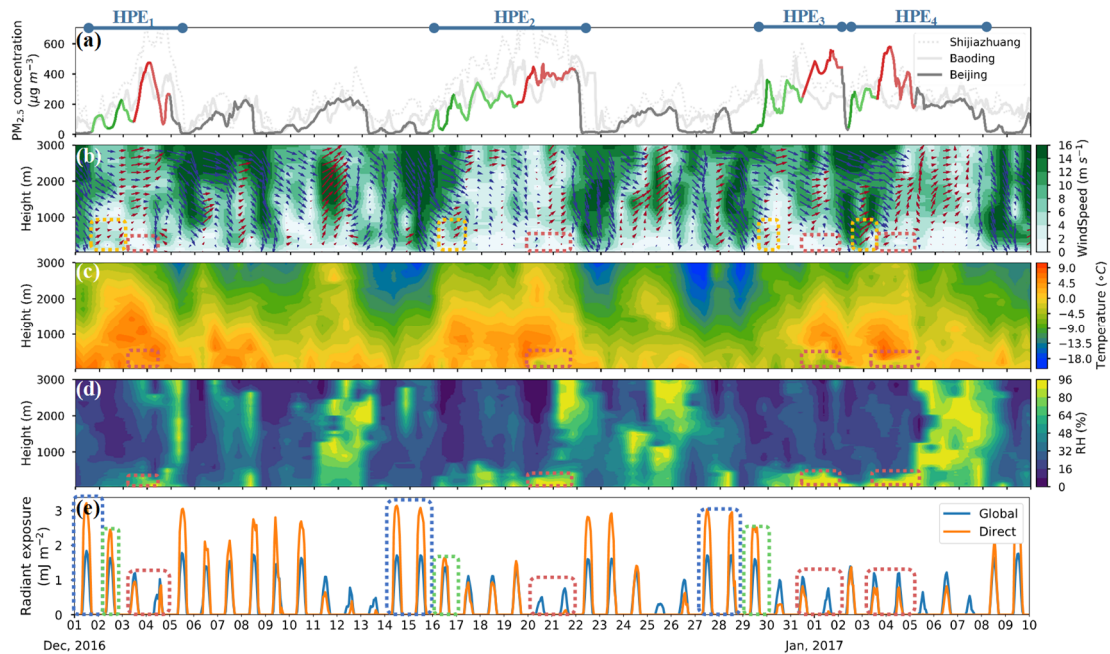
33 and the Northeast China Plain (NeCP). In this study, using surface PM_{2.5} and radiation observations,
34 radiosonde observations, and reanalysis data, we observed the existence of a two-way feedback
35 mechanism in the above six regions. In the SB, this two-way feedback mechanism is weak due to the
36 suppression of cloudy mid-upper layers. In the more polluted NCP, the GZP, and the NeCP, the feedback
37 is more striking than that in the YRD, the TLB, and the PRD. In these regions, the feedback of worsened
38 meteorological conditions on PM_{2.5} explains 60~70% of the increase in PM_{2.5} during the cumulative
39 stages (CSs). For each region, the low-level cooling bias becomes increasingly substantial with
40 aggravating aerosol pollution and a closer distance to the ground surface. With PM_{2.5} mass concentrations
41 greater than 400 $\mu\text{g m}^{-3}$, the near-ground bias exceeded -4 °C in Beijing and reached up to approximately
42 -4 °C in Xi'an; this result was caused by accumulated aerosol mass to some extent. In addition to the
43 increase in PM_{2.5} caused by the two-way feedback, these regions also suffer from the regional transport
44 of pollutants, including inter-regional transport in the GZP, trans-regional transport from the NCP to the
45 YRD and the TLB, and southwesterly transport in the NeCP.

46 **1 Introduction:**

47 In China, 94% of the total population is distributed in eastern China (Yang et al., 2016), in which
48 aerosol pollution has drawn wide attention. In the basins and plains in eastern China, aerosol pollution
49 episodes frequently occur in winter, and these episodes cause economic loss and have adverse effects on
50 human health (Bai et al., 2007; Matus et al., 2012; Chen et al., 2013). For example, in January 2013,
51 persistent heavy aerosol episodes affected 600 million people throughout 1.4 million square kilometers
52 (<http://www.infzm.com/content/95493>), which led to hundreds of flight cancellations and an increase in
53 the number of reported respiratory disease cases (Ji et al., 2014). During the wintertime (i.e., Jan., Feb.,
54 and Dec.) from 2013 to 2017, more than 28 persistent heavy aerosol pollution episodes that lasted for
55 more than 3 consecutive days (HPEs) occurred in Beijing; the peak value of particulate matter smaller
56 than 2.5 μm in diameter (PM_{2.5}) ranged from $\sim 200 \mu\text{g m}^{-3}$ to $\sim 800 \mu\text{g m}^{-3}$, with a mean duration longer
57 than 5 days (Zhong et al., 2018a; Zhong et al., 2019). The main cause of frequent pollution episodes is
58 the massive emissions of air pollutants produced by intense living and industrial activities in the basins
59 and plains (Zhang et al., 2009a; Zhang et al., 2012a; Zhang et al., 2013). In addition to pollutant emissions,
60 the relatively closed terrains of basins and plains limit the diffusion of aerosols and their precursors to

61 the surrounding areas (Su et al., 2004;Zhu et al., 2018). Under stable meteorological conditions, aerosol
62 pollution forms and further accumulates (Zhang et al., 2013;Zhong et al., 2017).

63 In winter, unfavorable meteorological conditions lead to aerosol pollution formation, and after
64 accumulating to some extent, aerosols will change the atmospheric structure by interacting with solar
65 radiation (Boucher et al., 2013b;Zhong et al., 2018b). The details of the two-way feedback mechanism
66 between unfavorable meteorological conditions and cumulative aerosols in Beijing are as follows: 1)
67 When upper zonal large-scale circulations unfavorable for pollution dispersion occur, the boundary layer
68 (BL) height reduces from ~ 1500 m in clean stages to 700-800 m; under the BL, the winds shift from
69 northerly to southerly, which transport pollutants from the south of Beijing (transport stages (TSs) in Fig.
70 1). Above unfavorable meteorological conditions cause aerosol pollution formation. 2). When the vertical
71 aerosols are accumulated to a certain degree, the dominant scattering aerosols will substantially back-
72 scatter solar radiation, causing a reduction in the amount of solar radiation that reaches the surface, which
73 causes a near-ground cooling effect through atmospheric circulation and vertical mixing (i.e., the
74 cumulative sum of hourly surface vertical and global radiant exposure reduced by 89% and 56%,
75 respectively, from clean stages to cumulative stages (CSs) (Fig.1)) (Zhong et al., 2017;Zhong et al.,
76 2018b). With less solar radiation, near-ground temperature subsequently decreases. 3).Under slight or
77 calm winds, the temperature reduction induces or reinforces an inversion that further weakens turbulence
78 diffusion and results in a lower BL height, which further worsens aerosol pollution (during CSs in Fig.1).
79 5). This condition also decreases the near-ground saturation vapor pressure and suppresses water vapor
80 diffusion to increase the relative humidity (RH), which will further enhances aerosol hygroscopic growth
81 and accelerates liquid-phase and heterogeneous reactions to worsen aerosol pollution (Pilinis et al.,
82 1989;Ervens et al., 2011;Kuang et al., 2016;Zhong et al., 2018b;Zhong et al., 2018a). This feedback
83 effect of further worsened meteorological conditions aggravates PM_{2.5} pollution (during CSs in Fig.1)
84 (Zhong et al., 2017).



85
 86 **Figure 1: Temporal variations in PM_{2.5}, surface radiation, and vertical distributions of**
 87 **meteorological factors from December 1, 2016, to January 10, 2017.** (a) PM_{2.5} mass concentration
 88 (gray or colored line: Beijing; light gray line: Baoding; gray dot: Shijiazhuang); (b) winds (vectors) and
 89 wind velocity (shadings; units: m s⁻¹); (c) temperature (shadings; units: °C); (d) RH (shadings; units: %);
 90 and (e) direct radiant exposure (of the vertical surface to the direction of solar radiation) and global
 91 radiant exposure. (Blue line: HPEs; green line and orange box: TSs; red line and white or red box: CSs;
 92 blue box: clean periods) (*Adapted from Zhong et al, 2018b*)

93 The two-way feedback mechanism between unfavorable meteorological conditions and cumulative
 94 aerosol pollution also appeared in other cities in the North China Plain, including Tangshan, Xingtai,
 95 Zhengzhou and Nanyang (Liu et al, 2018, under review). Whether the two-way feedback mechanism
 96 exists in other basins and plains in eastern China, which have weaker aerosol pollution than that in the
 97 North China Plain, is unclear. If such feedback exists, its magnitude requires further investigation.
 98 Currently, to the best of our knowledge, studies on the existence, magnitude, and comparison of the two-
 99 way feedback in these basins and plains are insufficient. Overall, we lack a comprehensive understanding
 100 of the feedback mechanism in China. Therefore, here we used surface PM_{2.5} mass concentrations,
 101 radiosonde observations of meteorological factors, meteorological index parameter-linking aerosol
 102 pollution and meteorological factors (PLAM), and ERA-interim reanalysis data from the European
 103 Center for Medium Weather Forecasting (ECMWF) to investigate the two-way feedback mechanism in
 104 the key regions of populous eastern China (Yang et al., 2016), including the Guanzhong Plain, the
 105 Yangtze River Delta, the Two Lakes Basin, the Pearl River Delta, the Sichuan Basin, and the Northeast
 106 China Plain, which are densely populated and economically developed regions that include massive

107 industrial pollution sources, agricultural pollution sources, motor vehicle pollution sources and domestic
108 pollution sources. In the above regions, heavy aerosol episodes often occur in the regional central cities
109 with denser populations and stronger pollutant emissions, including Xi'an, Nanjing, Shanghai, Wuhan,
110 Guangzhou, Chengdu, and Shenyang. In the above cities, the impact of aerosol pollution episodes on the
111 economy, society, and health is far-reaching. Therefore, we focus on the feedback mechanism in the
112 above cities to represent the overall conditions in the five major haze regions of China, namely, II) the
113 North China Plain (also called Hua Bei Plain) in N. China, plus the Guanzhong Plain; III) E. China with
114 the main body in the Yangtze River Delta area; V) S. China with the most areas of Guangdong and the
115 Pearl River Delta area; IV) The Sichuan Basin in S. W. China, and I) Northeast China Plain (Zhang et
116 al., 2012b) (Fig. 1).

117 **2 Materials and methods:**

118 **2.1 PM_{2.5} observations:**

119 Since January 2013, the Ministry of Environmental Protection has been monitoring the PM_{2.5} mass
120 concentrations in real time at over 1000 environmental monitoring stations established in different
121 regions of China. In this study, we used the hourly PM_{2.5} mass concentrations provided by the Ministry
122 of Environmental Protection from December 1, 2016 to January 10, 2017 and the respective averaged
123 PM_{2.5} mass concentrations of all the urban stations in Xi'an, Yuncheng, Shenyang, Chengdu, Wuhan,
124 Nanjing, Shanghai, Jinan, Guangzhou and Qingyuan. The in situ monitoring data of the hourly
125 concentrations of PM_{2.5}, PM₁₀, CO, NO₂, SO₂, and O₃ are acquired from the national air quality real-time
126 publishing platform (<http://106.37.208.233:20035>).

127 We also used an unmanned aerial vehicle to observe PM_{2.5} mass concentration at different heights
128 within 1 km every three hours in Nanjing from December 3 to 4, 2017. The data were obtained with the
129 UAV platform-CEEWA X8 (Nanjing CEEWA Intelligent Technology Co., Ltd., Nanjing, China), a six-
130 rotor industrial UAV carrying highly reliable, triple-redundant FC-IU3 flight control system (Zhou et al.,
131 2018). On the platform, a multiparameter atmospheric environment detector was equipped, which was
132 developed by Shenzhen TENGWEI Measurement and Control Technology Co., Ltd., Shenzhen, China
133 (Zhou et al., 2018). The experiment was performed on the Xianlin campus of Nanjing University. This
134 campus is located in the eastern suburb of Nanjing and surrounded by farmland, residential areas, and

135 small patches of forest and chemical plants. The experiment site was located on a playground without
136 tall structures surrounded.

137 **2.2 Meteorological radiosonde observations:**

138 In China, 120 stations have been observing vertical meteorological factors using L-band sounding
139 radars. Their accurately positioned radar systems collect reliable meteorological data each second; thus,
140 these data have high spatial and temporal resolutions (Tao, 2006). In this study, we used the L-band
141 sounding radar data from the meteorological stations in Xi'an, Shenyang, Chengdu, Wuhan, Nanjing,
142 Shanghai, and Qingyuan; these stations observed several meteorological factors, including wind,
143 temperature and RH, twice each day at 0800 (BJT) and 2000 (BJT) from December 1, 2016 to January
144 10, 2017. The meteorological factors were analyzed in detail below the height of 3 km. The heights from
145 the surface to 1 km, from 1 km to 2 km, and from 2 km to 3 km are termed the low-level, mid-level, and
146 upper-level heights, respectively. In addition, due to the lack of meteorological radiosonde observations
147 in Guangzhou, we supplemented related observations in its adjacent city, Qingyuan.

148 **2.3 Surface meteorological data:**

149 Since 2001, national weather stations have been conducting automatic hourly observations. Some
150 of the stations began to record observations every 5 and 10 minutes starting in 2011. This study used the
151 hourly meteorological observation data, including temperature, pressure, RH, wind, and visibility at the
152 National Automatic Weather Stations (AWS) provided by the National Meteorological Information
153 Center of China Meteorological Administration (NMICMA). The time range of the selected data is from
154 December 1, 2016, to January 10, 2017.

155 We also used an hourly radiant exposure data set of national meteorological radiation factors (V2.0)
156 provided by the NMICMA. This dataset contains 104 radiation stations, including primary stations with
157 global, direct, scattered, reflected, and net radiation, secondary stations with global and net radiation, and
158 tertiary stations with only global radiation. These radiation stations recorded hourly basic radiant
159 exposure data and the corresponding station information (i.e., latitude, longitude, and altitude) starting
160 in 1993. In this study, we used the global, direct and net radiant exposure from December 1, 2016, to
161 January 10, 2017.

162 **2.4 PLAM data**

163 Based on the definition and calculation formula of PLAM (a parameter that links aerosol
164 pollution and meteorological factors) (Zhang et al., 2009b; Wang et al., 2012; Wang et al.,
165 2013; Zhang et al., 2015), we obtained the PLAMs in Xi'an, Nanjing, Wuhan, Qingyuan, Chengdu,
166 and Shenyang using surface meteorological factors. PLAM includes two major separate factors: (1)
167 the initial meteorological conditions $\alpha(m)$ associated with the atmospheric condensation processes
168 and (2) an effective dynamic parameter associated with the initial contribution of air pollution $\beta(c')$:

$$169 \quad \text{PLAM} = \alpha(m) \times \beta'(c). \quad (1)$$

170 This calculation mainly indicates regional atmospheric stability and air condensation ability. The
171 details of the calculation have been presented in previous studies (Wang et al., 2012; Wang et al.,
172 2013).

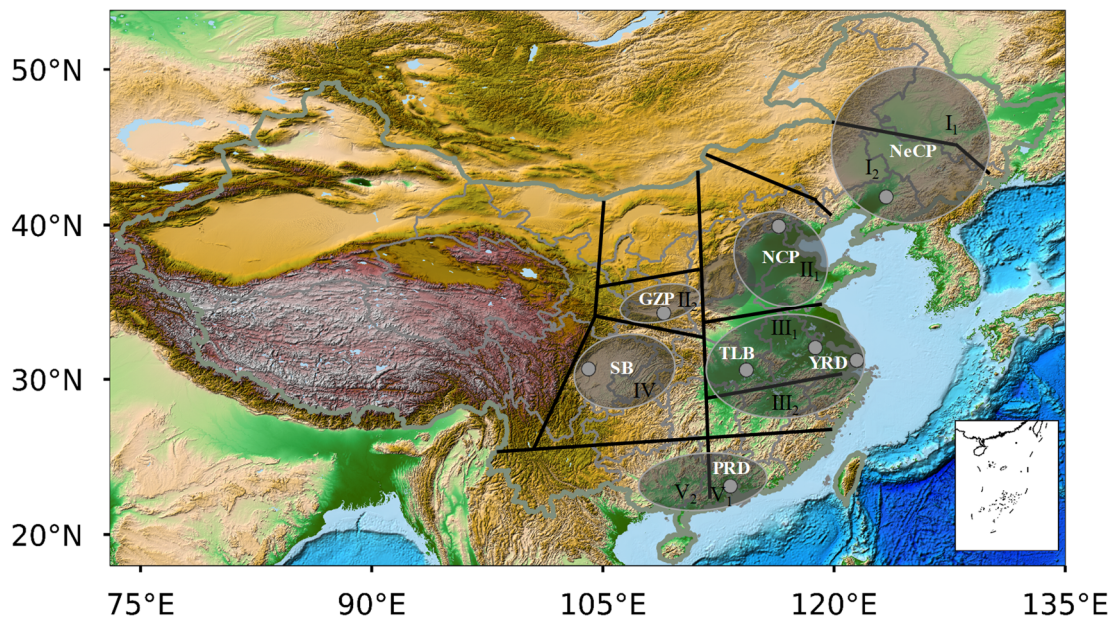
173 **2.5 ECMWF ERA-Interim data**

174 ERA-Interim is ECMWF's latest global atmospheric reanalysis, which extends back to 1979 and
175 continuously updates in real time (Dee et al., 2011). It is produced with a 4-dimensional variational data
176 assimilation scheme and advances forward in time using 12-hour analysis cycles (Thépaut et al.,
177 1996; Dee et al., 2011). Before assimilation, all data are subject to gross, redundancy and background
178 quality controls, which resulted in a large drop between the total number of available data and the number
179 of data used in the assimilation. The mean daily usage rate of radiosondes is no more than 50% over the
180 entire period (Poli et al., 2010). In addition, although the effect of aerosols on radiative transfer in the
181 atmosphere is modeled based on prescribed climatological aerosol distributions (Dee et al., 2011), it has
182 not considered the two-way feedback mechanism between the cumulated aerosol pollution and the
183 worsened meteorological conditions (Simmons, 2006). Therefore, the magnitude of the feedback
184 mechanism could be statistically reflected by the gaps between the ERA-interim reanalysis and the
185 meteorological radiosonde observations. The disparities have been used to present the observational
186 evidence of aerosol-PBL interactions in Beijing (Ding et al., 2016; Huang et al., 2018).

187 In this study, we used ERA-Interim data with a horizontal resolution of $0.125^\circ \times 0.125^\circ$. Its
188 mandatory pressure levels include 1000, 975, 950, 925, 900, 875, 850, 825, 800, 775, 750, and 700 hPa.
189 According to these pressure layers, we interpolated the radiosonde observations and calculated the
190 vertical temperature differences between the ERA-interim reanalysis and the interpolated sounding data
191 at 20:00 (BJT).

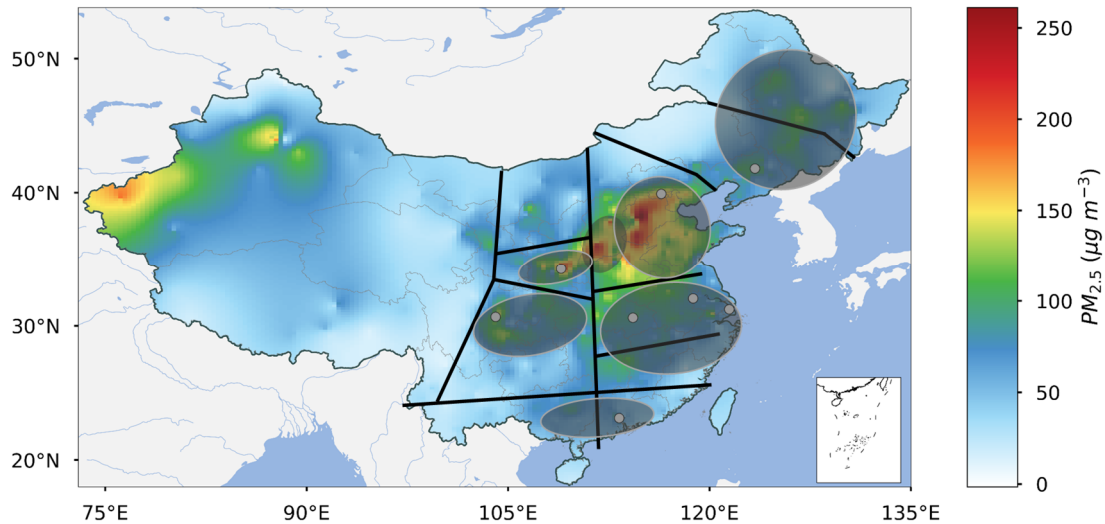
192 **3 Results and Discussions:**

193 Based on the consistent variation trends in visibility, China is classified into nine typical regions
194 (Zhang et al., 2012b). Five of these regions have experienced striking declines in visibility in recent
195 decades, including (1) the North China Plain and the Guanzhong Plain in North China; (2) the Yangtze
196 River Delta region and the Two Lakes Basin along the middle and lower reaches of the Yangtze River;
197 (3) the Pearl River Delta region in South China; (4) the Sichuan Basin in Southwest China; (5) and the
198 Northeast China Plain (Fig. 2). The areas with declined visibility coincide with the basins and plains in
199 eastern China because these basins and plains are densely populated and topographically enclosed;
200 additionally, these areas emit and produce massive air pollutants, including primary aerosols and
201 secondary aerosols from gas-to-particle conversion. These aerosols locally accumulate to continuously
202 reduce visibility. By comparing the mean PM_{2.5} mass concentration from December 1, 2016 to that of
203 January 10, 2017 in the five regions that experienced declines in visibility (Fig. 3), we found that the
204 heaviest aerosol pollution occurred in the North China Plain, and it was followed by the Guanzhong Plain.
205 The areas with the next highest aerosol pollution were the Sichuan Basin and the Northeast China Plain.
206 The Two Lakes Basin and the Yangtze River Delta experienced less aerosol pollution. Finally, the Pearl
207 River Delta had the least aerosol pollution.



208
209 **Figure 2: The key haze regions with similar declines in visibility in eastern China.** (White dot: locations of
210 radiosonde stations)

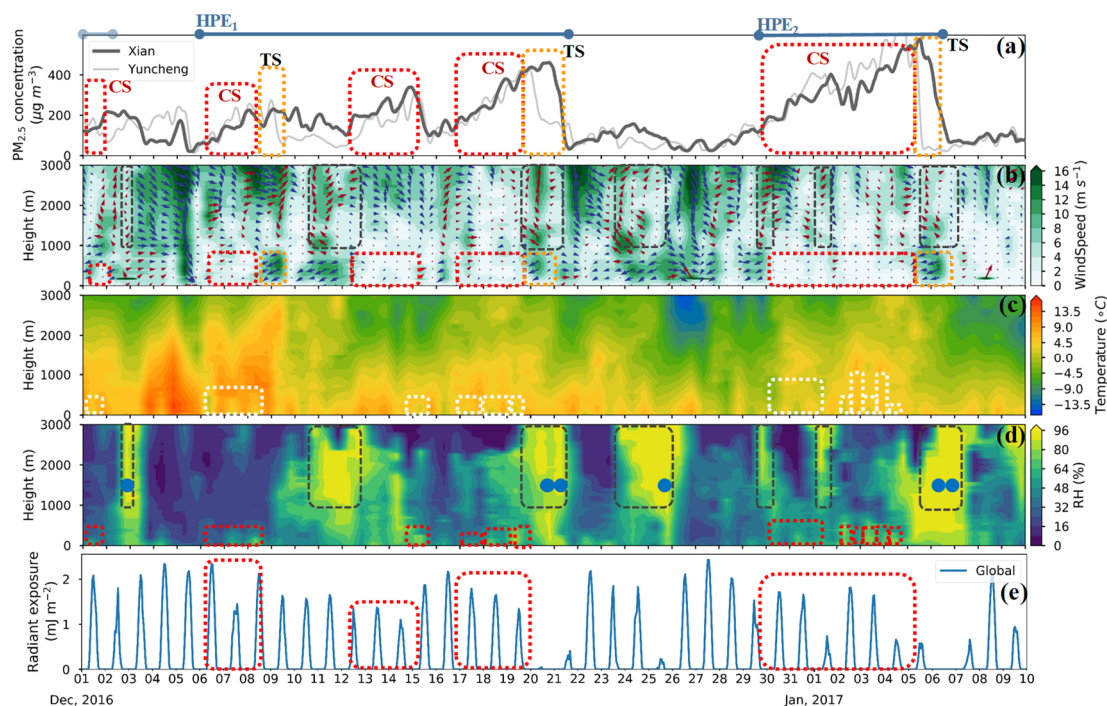
211



212
 213 **Figure 3: National distribution of mean PM_{2.5} mass concentration from December 1, 2016, to January 10,**
 214 **2017. (White dot: locations of radiosonde stations)**

215 **3.1 Striking two-way feedback in the polluted Guanzhong Plain with inter-regional pollution**
 216 **transport.**

217 To the north of the Loess Plateau and the south of the Qinling Mountains, the Guanzhong Plain has
 218 a narrow and closed terrain (Fig. 2), and its climatic and meteorological conditions are distinctive from
 219 those of the surrounding areas. Compared with the plateau to the north, the Guanzhong Plain is less
 220 affected by northerly cold and clean winds, and these conditions favor the accumulation of pollutants.
 221 However, because the Loess Plateau is lower in elevation than the Hengduan Mountains and the Daba
 222 Mountains located to the northwest of the Sichuan Basin, the barrier effect of the plateau on the northerly
 223 cold air is weaker than that of those mountains (Fig. 4 (b) and Fig. 12 (b)). Because the North China
 224 Plain is bordered to the west by the Taihang Mountains and the Lvliang Mountains (Fig. 2), the
 225 Guanzhong Plain is rarely affected by pollutant transport from the North China Plain; however, air
 226 pollution is highly correlated among the different cities in the Guanzhong Plain. To the west of this plain,
 227 Xi'an lies north of the Wei River and the Loess Plateau and south of the Qinling Mountains (Fig. 2). Due
 228 to its enclosed topography, Xi'an frequently experiences heavy urban aerosol pollution.



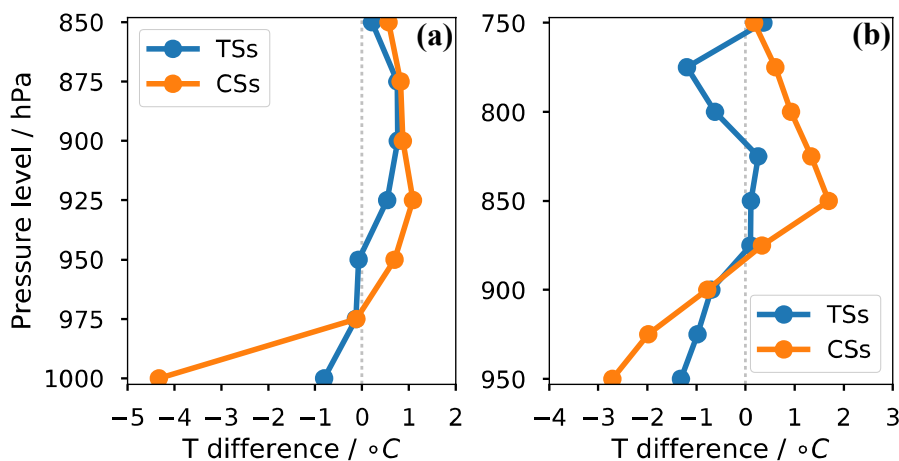
229
230 **Figure 4: Temporal variations in PM_{2.5}, surface radiation, and vertical distributions of meteorological**

231 **factors from December 1, 2016, to January 10, 2017.** (a) PM_{2.5} mass concentration (gray line: Beijing; light gray
232 line: Yuncheng); (b) winds (vectors) and wind velocity (shadings; units: m s⁻¹); (c) temperature (shadings;
233 units: °C); (d) RH (shadings; units: %); and (e) global radiant exposure. (Blue line: HPEs; light blue line: PEs;
234 white or red box: CSs; and brown box: water vapor transport)

235 From December 1, 2016, to January 10, 2017, two HPEs appeared in Xi'an and persisted for more
236 than 7 days with peak mass concentrations greater than 400 μg m⁻³ (Fig. 4 (a), dark blue lines). During
237 HPE₁₋₂, we observed a striking two-way feedback mechanism between the worsened weather conditions
238 and the cumulated aerosol pollution (Fig. 4, red and white boxes). When the near-ground PM_{2.5}
239 accumulates to a certain extent, the particles scatter more solar radiation back to space, which
240 substantially reduces the surface radiation (Fig. 4 (e), red boxes) and consequently lowers the near-
241 surface temperature (Fig. 4 (c), white boxes). Under slight or calm winds (Fig. 4 (b), red boxes), the
242 temperature reduction induces or reinforces inversions, which further weaken turbulence diffusion to
243 suppress the diffusion of water vapor and pollutants (Zhong et al., 2017; Zhong et al., 2018a); these
244 conditions also decrease the near-ground saturation vapor pressure to increase the RH (Fig. 4 (d), red
245 boxes), which further enhances aerosol hygroscopic growth and accelerates liquid-phase and
246 heterogeneous reactions (Cheng et al., 2016; Fang et al., 2016; Tie et al., 2017). This type of two-way
247 feedback mechanism leads to worsened meteorological conditions and elevated PM_{2.5} mass
248 concentrations.

249 To quantify the magnitude of the two-way feedback during TSs and CSs in polluted Beijing and

250 Xi'an, we obtained the air temperature difference between the radiosonde observations at 2000 BJT
 251 affected by this two-way feedback (whose temperature profiles were more affected by aerosols' blocking
 252 in solar radiation transfer compared with observations at 0800 BJT) and the ERA-interim reanalysis data
 253 without the feedback. We found that the temperature profile was modified by aerosols during both the
 254 TSs and the CSs in Beijing and Xi'an (Fig.5 (a, b)). However, a comparison of aerosol-induced
 255 temperature modification in the TSs and the CSs indicates that the lower cooling bias was more striking
 256 in the CSs, which also became increasingly substantial with a closer distance to the ground surface. From
 257 TSs to CSs, the negative temperature difference at 1000 hPa increased from -0.8 °C to -4.3 °C and
 258 from -1.3 °C to -2.7 °C in Beijing and Xi'an respectively. Using the near-ground temperature reduction
 259 (1000 hPa) as an index to evaluate the magnitude of the two-way feedback from TSs to CSs, we found
 260 that during TSs the aerosol-induced cooling bias was 18.6% and 48.7% of the difference during CSs in
 261 Beijing and Xi'an respectively. It is expectable because from the TSs to the CSs aerosol pollution
 262 worsened with increasing radiative cooling effects. Moreover, though relatively strong winds in the TSs
 263 were conducive to pollution transport, they were unfavorable for the formation and maintenance of stable
 264 stratification, in which occurred aerosol self-induced pollution deterioration frequently.



265
 266 **Figure 5: Vertical mean temperature difference between sounding observations and ERA-interim reanalysis**
 267 **data during TSs and CSs from December 1, 2016, to January 10, 2017. (a) Beijing; (b) Xi'an**

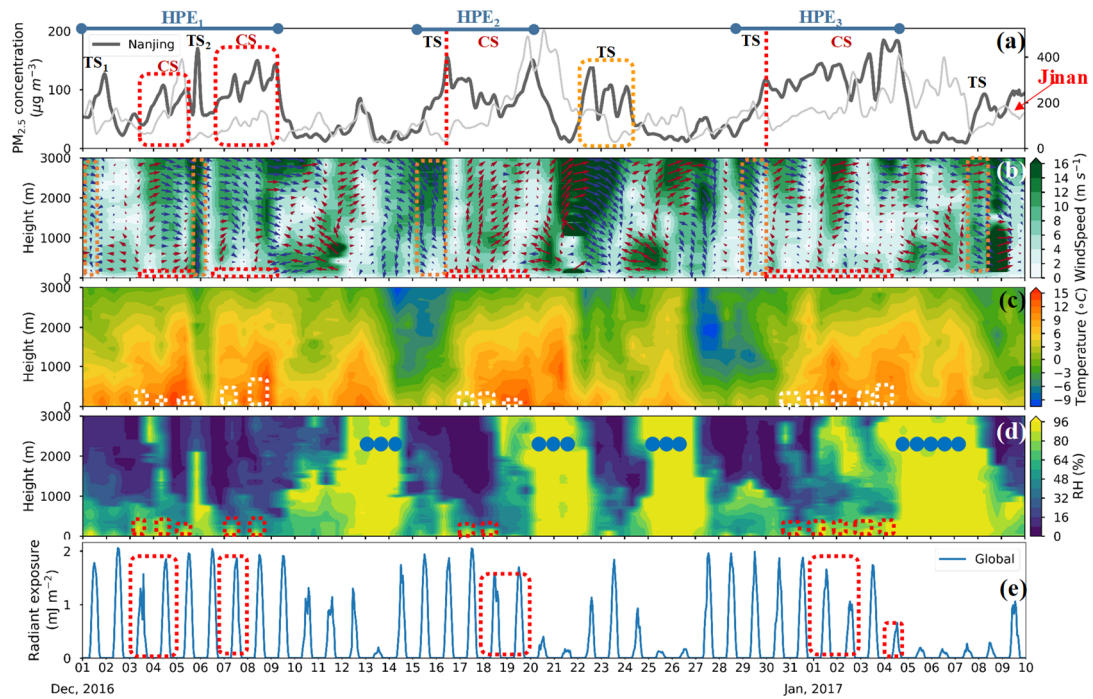
268 During HPE₁₋₂, we also observed an increase in the PM_{2.5} mass concentration caused by pollutant
 269 transport. The aerosol pollution in Xi'an might be aggravated by the transport of pollutants from the
 270 eastern polluted plain area with heavily polluted cities, including Yuncheng and Linfen. To reveal the
 271 effects of air pollutant transport from the eastern plain on the aerosol pollution in Xi'an, we compared
 272 the variation trends in the PM_{2.5} mass concentrations in Xi'an and Yuncheng under lower northwesterly

273 winds (Fig. 4 (a, b)). We found that during TSs in Fig. 4 (orange boxes), low-level northwesterly winds
274 would transport pollutants below the BL to maintain or aggravate the aerosol pollution in Xi'an when
275 Yuncheng is heavily polluted; however, when Yuncheng had good air quality, the aerosol pollution in
276 Xi'an was lighter or even eliminated.

277 In addition to the scavenging effect of clean northwesterly winds on aerosol pollution, pollution
278 elimination mainly depends on lower strong northwesterly winds and mid-upper level southerly winds.
279 Because the Loess Plateau north of Xi'an is sparsely populated with rare air pollutant emissions, lower
280 strong and clean northwesterly winds would blow away aerosol pollutants in Xi'an, causing a subsequent
281 rapid improvement in the air quality (Fig. 4 (a, b)). Since the mid-upper level southerly winds transport
282 water vapor to Xi'an from the area south of Xi'an, the mid-upper (or whole-layer) RH level is
283 considerably enhanced (i.e., greater than 96%) (Fig. 4 (b, d), brown boxes), which causes the PM_{2.5} to
284 enter the fog-cloud phase and possibly produces precipitation that eliminates pollutants through wet
285 removal (Fig. 4 (d), blue dots represent precipitation).

286 **3.2 Affected by trans-regional pollution transport from the North China Plain, the Yangtze River** 287 **Delta region subsequently experiences the two-way feedback.**

288 Located in the lower reaches of the Yangtze River, the Yangtze River Delta is a triangle-shaped
289 metropolitan region. It covers an area of 211,700 km² and is home to more than 150 million people as
290 of 2014 (http://www.ndrc.gov.cn/zcfb/zcfbghwb/201606/t20160603_806390.html). The urban build-up
291 in this area has given rise to what may be the largest concentration of adjacent metropolitan areas in the
292 world. The Yangtze River Delta has a marine monsoon subtropical climate with cool and dry winters.
293 Situated in the Yangtze River Delta, Nanjing is the second largest city in the East China region. The south,
294 north, and east sides of the city are surrounded by the Ningzheng Ridges (Fig. 2), while the Yangtze River
295 flows along the west and part of the north sides.



296

297

Figure 6: Temporal variations in PM_{2.5}, surface radiation, and vertical distributions of meteorological

298

factors from December 1, 2016, to January 10, 2017. (a) PM_{2.5} mass concentration (gray line: Nanjing; light

299

gray line: Jinan); (b) winds (vectors) and wind velocity (shadings; units: m s⁻¹); (c) temperature (shadings;

300

units: °C); (d) RH (shadings; units: %); and (e) global radiant exposure. (Blue line: HPEs; light blue line: PEs;

301

white or red box: CSs; and blue dot: precipitation.)

302

From December 1, 2016, to January 10, 2017, four aerosol pollution episodes occurred in Nanjing

303

(Fig. 6 (a), blue boxes). One of these episodes lasted for less than 3 days and had light pollution, while

304

the other three episodes persisted for more than 5 days and had peak mass concentrations greater than

305

150 µg m⁻³; thus, these three episodes are termed HPEs (Fig. 6 (a)). During these three HPEs, although

306

the PM_{2.5} mass concentration was much lower than that in Beijing, the aerosol pollution formation was

307

similar to that in the latter, including earlier TSs and later CSs (Zhong et al., 2017; Zhong et al., 2018a).

308

During the TSs in the HPEs, strong northerly winds transport aerosol pollutants from the polluted North

309

China Plain to the Yangtze River Delta region below and over the BL (i.e., long-distance pollution

310

transport), which induces a striking increase in the PM_{2.5} mass concentration in Nanjing and a reduction

311

in the PM_{2.5} mass concentration in Jinan, a regional center city representative of the pollution conditions

312

in the NCP (Fig. 6 (a, b)). To some extent, based on the PM_{2.5} mass, the two-way feedback mechanism

313

is activated during the CSs, in which we observed surface radiation reductions, near-surface inversions,

314

low-layer RH enhancement, and increased PM_{2.5} mass concentrations under slight winds (Fig. 6). Due to

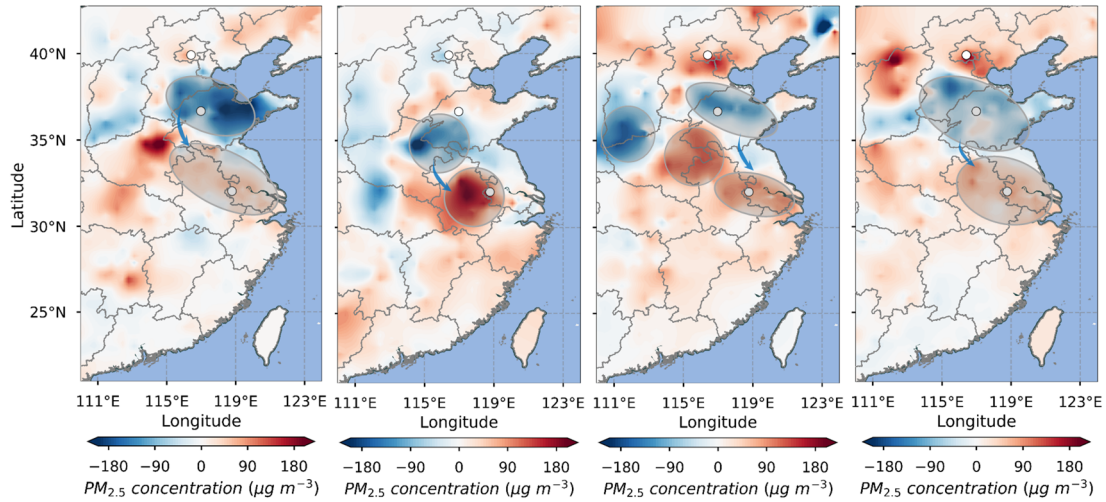
315

the lighter aerosol pollution in Nanjing, the two-way feedback mechanism is weaker than that in Beijing

316

(Fig. 1, 6 (a)). In addition, the mechanism might be weakened by relatively strong lower winds (compared

317 to those in Beijing) (Fig. 1, 6 (b)), which are unfavorable for the accumulation of aerosols.

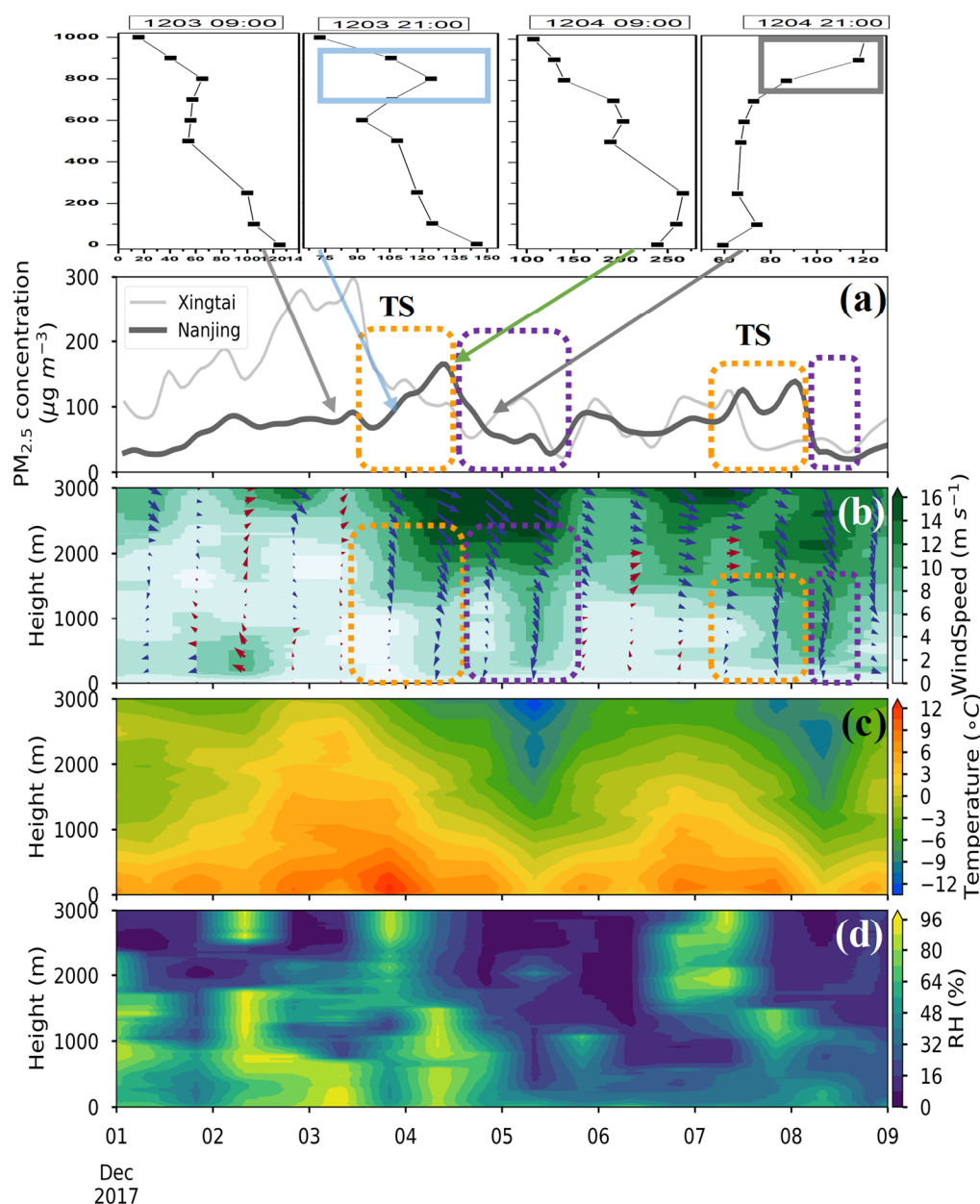


318

319 **Figure 7: The distribution of the concentration differences in PM_{2.5} mass between the start time and the end**
320 **time (the end is subtracted from the start) of the TSs in Figure 4. (a) TS₁ in HPE₁; (b) TS₂ in HPE₁; (c) TS in**
321 **HPE₂; and (d) TS in HPE₃.**

322

To reveal the regional pollutant transport patterns from the North China Plain to the Yangtze River
323 Delta region, we calculated the concentration difference in the PM_{2.5} mass between the start time and the
324 end time of the TSs in HPE_{1,2,4} (Fig. 7). We found that the southern area of the North China Plain
325 experienced a substantial reduction in its PM_{2.5} mass concentration, while an increase occurred in the
326 middle and lower reaches of the Yangtze River, including the Two Lakes Basin and the Yangtze River
327 Delta region; these results indicate the process of regional pollutant transport from the North China area
328 to the East China area under strong northwesterly winds. In the winter of 2017, we also observed this
329 pollution transport (Fig. 6, orange boxes), As shown in Fig. 8, we observed mid-level pollutants transport
330 at the beginning of the TS, after which near-surface PM_{2.5} reaches the highest concentration with
331 downward mixing. Subsequently, another northerly pollutant transport reached middle layers over
332 Nanjing. Afterward, persistent northerly winds blew pollutants away (Fig. 8, purple boxes). In addition
333 to the blowing effect of persistent northerly winds, eliminating pollution in Nanjing mainly depends on
334 strong southeasterly winds, which transport warm, humid, and clean air from the Yellow Sea and the East
335 China Sea; this air also blows the aerosol pollutants in Nanjing away (Fig. 6 (b, c, d)). In addition,
336 transported water vapor increases the RH (Fig. 6 (b, d)), which causes the PM_{2.5} to enter the fog-cloud
337 phase and possibly produces precipitation that eliminates pollutants through wet removal (Fig. 6 (d), blue
338 dots represent precipitation).

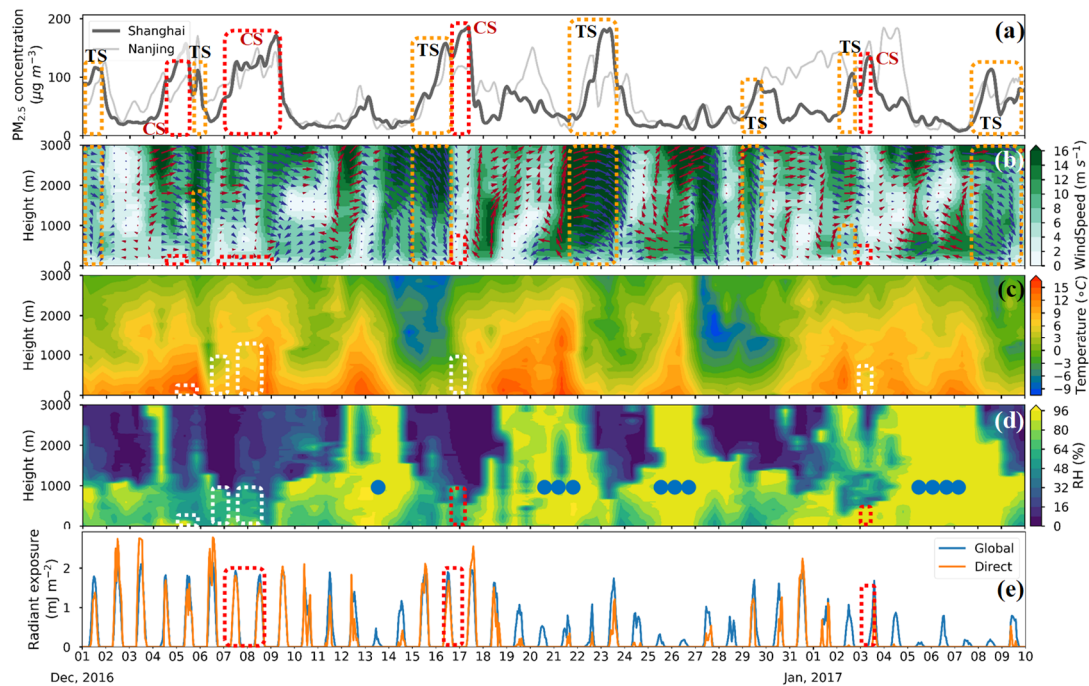


339

340 **Figure 8: Temporal variations in PM_{2.5} and vertical distributions of meteorological factors from December**
 341 **1, 2017 to December 9, 2017.** (a) PM_{2.5} mass concentration (gray line: Nanjing; light gray line: Xingtai); (b)
 342 winds (vectors) and wind velocity (shadings; units: m s^{-1}); (c) temperature (shadings; units: $^{\circ}\text{C}$); and (d) RH
 343 (shadings; units: %). (Orange box: TSs; purple box: clean periods)

344 Consistent with the results observed in Nanjing, Shanghai also experienced long-distance pollution
 345 transport below and over the BL under northwesterly winds (Fig. 9 (a, b), orange boxes). After PM_{2.5}
 346 accumulated to some extent, we observed a two-way feedback mechanism, including reduced radiation,
 347 near-surface inversions, RH enhancement in the lower parts of BL, and increase in PM_{2.5} mass
 348 concentration under slight or calm winds (Fig. 9 (a, b, c, d, e) red and white boxes); however, the
 349 magnitude of the feedback was weaker than that observed in Nanjing (Fig. 6). Because Shanghai is closer

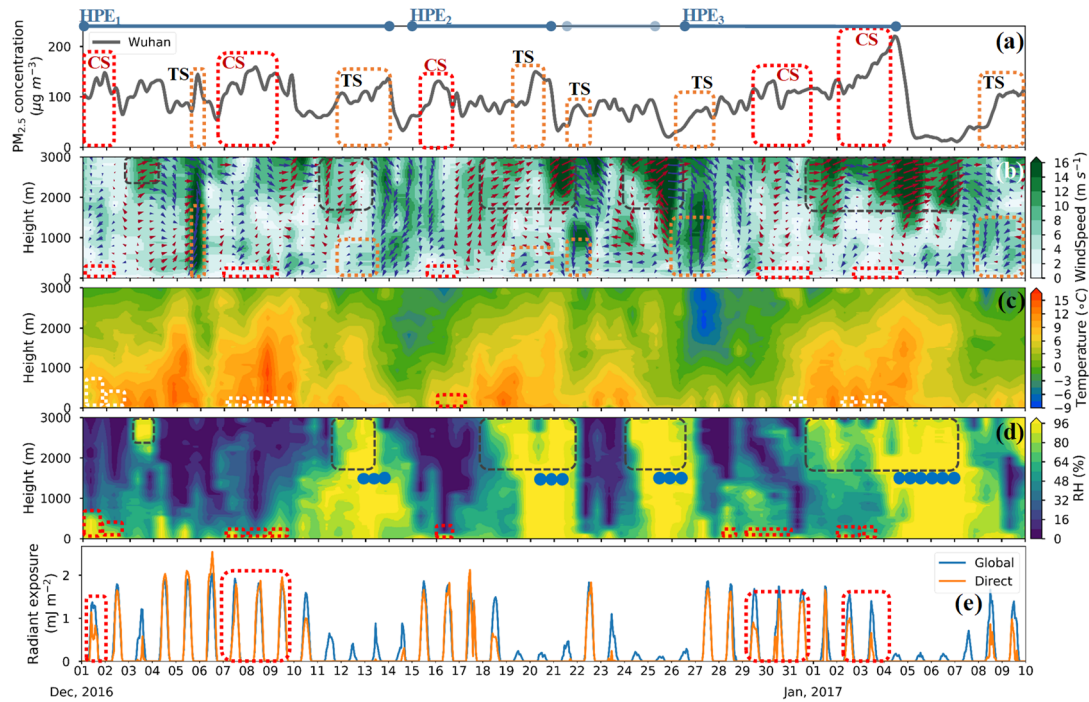
350 to the sea than Nanjing, it is more susceptible to warm, humid southeasterly winds from the sea, which
 351 carry more water vapor to Shanghai than to Nanjing (Figs. 6 & 9 (b, d)).



352
 353 **Figure 9: Temporal variations in PM_{2.5}, surface radiation, and vertical distributions of meteorological**
 354 **factors from December 1, 2016, to January 10, 2017.** (a) PM_{2.5} mass concentration (gray line: Shanghai; light
 355 gray line: Nanjing); (b) winds (vectors) and wind velocity (shadings; units: m s⁻¹); (c) temperature (shadings;
 356 units: °C); (d) RH (shadings; units: %); and (e) direct radiant exposure (of the vertical surface to the direction of
 357 solar radiation) and global radiant exposure. (White or red box: CSs; orange box: TSs; and blue dot: precipitation)

358 **3.3 The two-way feedback exists in the Two Lakes Basin, in which aerosol pollution is also**
 359 **worsened by the trans-regional pollution transport from the North China Plain.**

360 The Two Lakes Basin is in the middle reaches of the Yangtze River. With the Sichuan Basin
 361 bordered to the northwest by the Daba Mountains (Fig. 2), the Two Lakes Basin is rarely affected by
 362 pollutant transport from polluted cities in Sichuan Basin. The north side of the Two Lakes Basin is
 363 connected to the North China Plain through the Suizhou Corridor and the Nanyang Basin (Fig. 2); thus,
 364 the Two Lakes Basin is vulnerable to pollution transport from the North China Plain, which experiences
 365 the heaviest aerosol pollution in China (Fig. 3). As a large exorheic basin surrounded by low ridges or
 366 mountains, the Two Lakes Basin more frequently exchanges air masses with its surroundings, with wind
 367 speeds much higher than those in Sichuan Basin. Situated in the eastern Two Lakes Basin, Wuhan is the
 368 most populous city in Central China. The Yangtze and Han rivers wind through this city, which has a
 369 southern hilly and middle flat terrain (Fig. 2).



370
371
372
373
374
375
376

Figure 10: Temporal variations in PM_{2.5}, surface radiation, and vertical distributions of meteorological factors from December 1, 2016 to January 10, 2017. (a) PM_{2.5} mass concentration (gray line: Wuhan); (b) winds (vectors) and wind velocity (shadings; units: m s⁻¹); (c) temperature (shadings; units: °C); (d) RH (shadings; units: %); and (e) direct radiant exposure (of the vertical surface to the direction of solar radiation) and global radiant exposure. (Blue line: HPEs; light blue line: PEs; white or red box: CSs; orange box: TSs; brown box: water vapor transport; and blue dot: precipitation.)

377
378
379
380
381
382
383
384

From December 1, 2016 to January 10, 2017, four aerosol pollution episodes occurred in Wuhan (Fig. 10 (a), blue boxes). Three of these episodes lasted longer than 5 days and had peak mass concentrations greater than 150 μg m⁻³, which are termed HPEs (Fig. 10 (a)). During these three HPEs, we observed a two-way feedback mechanism in the red boxes (Fig. 10), including surface radiation reductions, near-surface inversions, low-level RH enhancement, and increases in PM_{2.5} mass concentrations under slight or calm winds (Fig. 10). Similar to the conditions observed in Nanjing, Wuhan experienced lighter aerosol pollution than Beijing (Fig. 1, 10 (a)); thus, the two-way feedback mechanism is weaker than that observed in Beijing.

385
386
387
388
389
390

Figure 7 shows the regional pollutant transport from the North China Plain to the Two Lakes Basin, which also aggravates the PM_{2.5} pollution in Wuhan. As shown in the orange boxes of Fig. 10, the lower northerly winds transport pollutants from the north of Wuhan to below Wuhan and sometimes over the BL, which results in increasing PM_{2.5} mass concentrations. Therefore, favorable northerly winds establish a pollution linkage between the North China Plain and the middle and lower reaches of the Yangtze River (including the Yangtze River Delta and the Two Lakes Basin), which have low and flat

391 terrains (Fig. 2). However, if the northerly winds are persistent and strong enough, they will blow the
392 aerosol pollutants out of the North China Plain entirely and then transport clean and cold winds to Wuhan;
393 under these conditions, the PM_{2.5} mass concentration first increases and then decreases dramatically. This
394 phenomenon was observed from December 12 to 14, 2016 and is shown in Fig. 10.

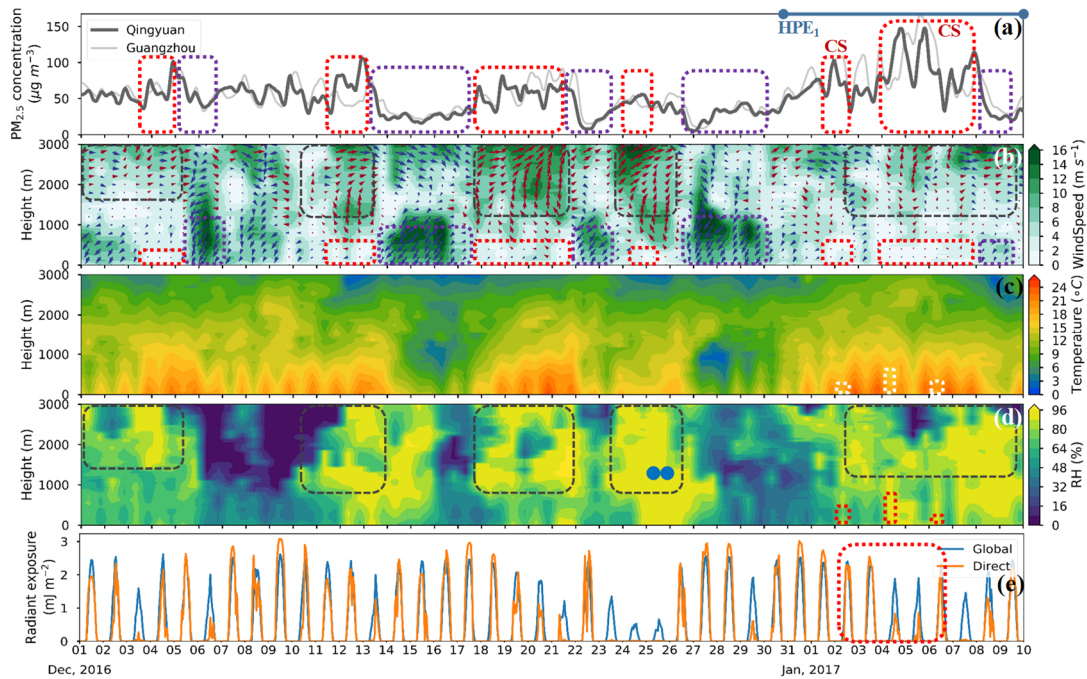
395 In addition to the blowing effect of the strong, persistent northerly winds, clearing the pollution in
396 Wuhan mainly depends on the mid-upper level southerly winds, particularly the southwesterly winds,
397 which transport water vapor to Wuhan from the south, substantially enhancing the RH (over 96%) (Fig.
398 10 (b, d), brown boxes); these conditions cause the PM_{2.5} to enter the fog-cloud phase and often produce
399 precipitation that eliminates pollutants through wet removal (Fig. 10 (d), blue dots represent
400 precipitation).

401 **3.4 The two-way feedback in the less polluted Pearl River Delta region, which is also humidified**
402 **by upper southerly winds from the South China Sea and purified by lower clean, cold**
403 **northeasterly winds.**

404 Located in the southeastern area of Guangdong Province, the Pearl River Delta is one of the most
405 populous and densely urbanized regions in the world. This low-lying area is surrounded by the Pearl
406 River estuary, where the East River, West River, and North River converge to flow into the South China
407 Sea. With the South China Sea to its south, the Pearl River Delta region is often influenced by southerly
408 sea winds; however, with the mountainous area in northern Guangdong to the north (Fig. 2), the Pearl
409 River Delta region is less affected by northerly cold and clean winds. Situated at the heart of the Pearl
410 River Delta region (Fig. 2), Guangzhou is the most populous city of Guangdong Province. However, due
411 to the lack of a meteorological radiosonde station in Guangzhou, we used the sounding observations from
412 Qingyuan, a city with similar PM_{2.5} variation trends (Fig. 9 (a)); Qingyuan is located approximately 60
413 km to the north of Guangzhou.

414 From December 1, 2016, to January 10, 2017, the PM_{2.5} mass concentration in Guangzhou and
415 Qingyuan is ~50 $\mu\text{g m}^{-3}$, which is much lower than that in Xi'an, Nanjing, Wuhan, Chengdu, and
416 Shenyang. During this period, only one HPE occurred, and it lasted for more than 8 days with a peak
417 mass concentration of approximately 150 $\mu\text{g m}^{-3}$ (Fig. 11, blue line). During this episode, we observed
418 surface radiation reductions, near-surface inversions, low-level RH enhancement, and increases in the
419 PM_{2.5} mass concentration under slight or calm winds (Fig. 11, red/white boxes below the blue line),

420 which suggest that a two-way feedback mechanism exists in the region. Except for this episode, we found
 421 that the PM_{2.5} mass concentration increased during slight or calm winds but was still below the threshold
 422 (Fig. 11, the red boxes before Jan 1, 2017) (Zhong et al., 2019); thus, no inversion or increased RH
 423 occurred because the two-way feedback mechanism was not effectively activated.



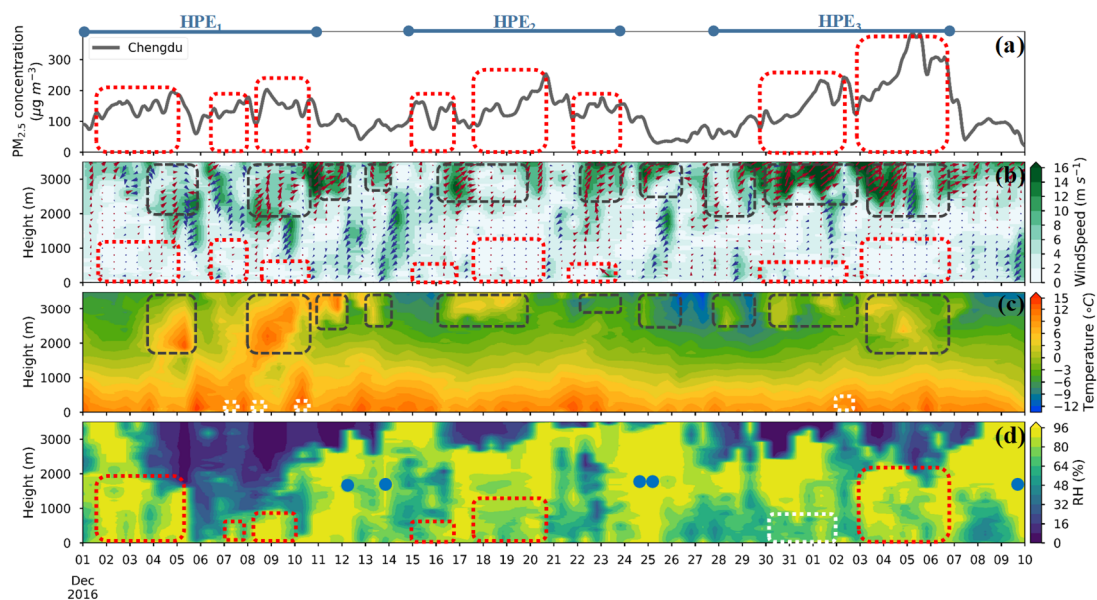
424
 425 **Figure 11: Temporal variations in PM_{2.5}, surface radiation, and vertical distributions of meteorological**
 426 **factors from December 1, 2016 to January 10, 2017.** (a) PM_{2.5} mass concentration (gray line: Qingyuan; light
 427 gray line: Guangzhou); (b) winds (vectors) and wind velocity (shadings; units: m s⁻¹); (c) temperature (shadings;
 428 units: °C); (d) RH (shadings; units: %); and (e) direct radiant exposure (of the vertical surface to the direction of
 429 solar radiation) and global radiant exposure. (Blue line: HPEs; white or red box: CSs; purple box: clearing; brown
 430 box: water vapor transport; and blue dot: precipitation)

431 Clearing pollution from Qingyuan depends on the lower strong northeasterly winds, which transport
 432 dry, cold, and clean air to decrease temperature and RH and blow aerosol pollutants away from Qingyuan.
 433 (Fig. 11 (b, d), purple boxes). In addition to the blowing effect of the cold northeasterly winds, the aerosol
 434 pollution in Qingyuan is also affected by the mid-upper level sea flows, which enhance the atmospheric
 435 RH to cause the PM_{2.5} to enter the fog-cloud phase and possibly produce precipitation that eliminates
 436 pollutants through wet removal (Fig. 11 (d), blue dots represent precipitation).

437 **3.5 The two-way feedback is weakened by cloudy mid-upper layers in the humid Sichuan Basin.**
 438 **This area is capped by upper-level inversions caused air moving east across the Tibet Plateau.**

439 Located in the upper reaches of the Yangtze River in southwestern China, the Sichuan Basin is a
 440 lowland region surrounded by mountains on all sides (Fig. 2). Abutting the eastern edge of the Tibetan

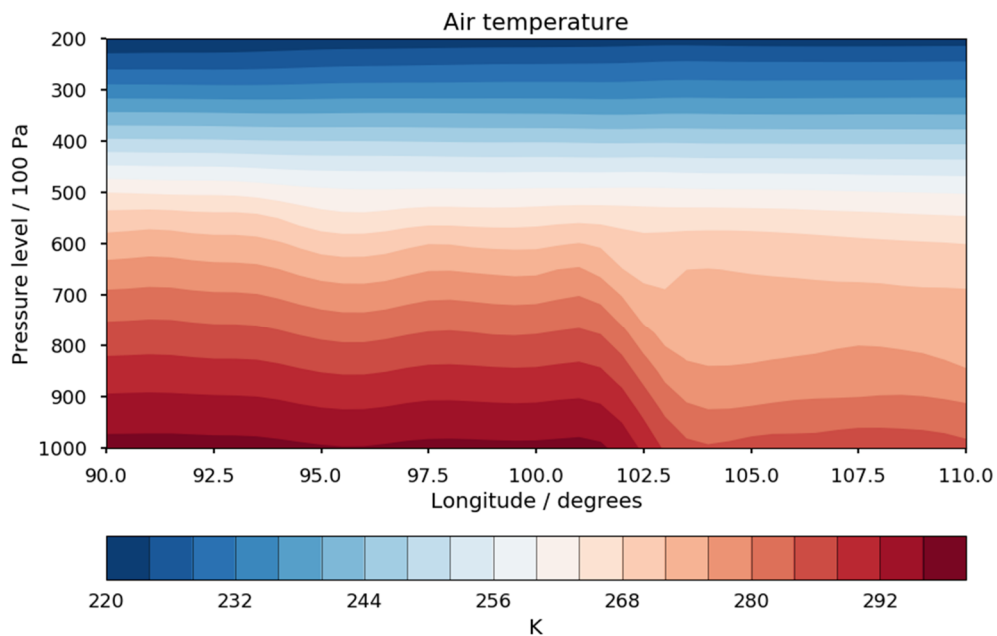
441 Plateau to the west and northwest and the Daba Mountains and the Wu Mountains to the east and
 442 northeast, respectively (Fig. 2), the Sichuan Basin is rarely affected by cold northerly winds, which are
 443 blocked by the high mountains. On the southern and southeastern sides, the Sichuan Basin is flanked by
 444 the lower Yungui Plateau (Fig. 2), which is frequently affected by warm, humid southwesterly and
 445 southeasterly airflows from the Bay of Bengal and the southeastern sea. Transported water vapor from
 446 the south is blocked by the tall northern mountains and then accumulates in the Sichuan Basin. Located
 447 at the western edge of the Sichuan Basin, Chengdu is surrounded by the highlands to the south, the high
 448 and steep Longmen Mountains to the northwest, the Qionglai Mountains to the west, and the low
 449 Longquan Mountains to the east. The enclosed topographical features lead to a lower wind speed and a
 450 higher RH in Chengdu than in other parts of the Sichuan Basin.



451
 452 **Figure 12: Temporal variations in PM_{2.5}, surface radiation and vertical distributions of meteorological**
 453 **factors from December 1, 2016, to January 10, 2017.** (a) PM_{2.5} mass concentration (gray line: Chengdu); (b)
 454 winds (vectors) and wind velocity (shadings; units: m s⁻¹); (c) temperature (shadings; units: °C); (d) RH (shadings;
 455 units: %); and. (Blue line: HPEs; white or red box: CSs; brown box: warm air flow or inversions; and blue dot:
 456 precipitation.)

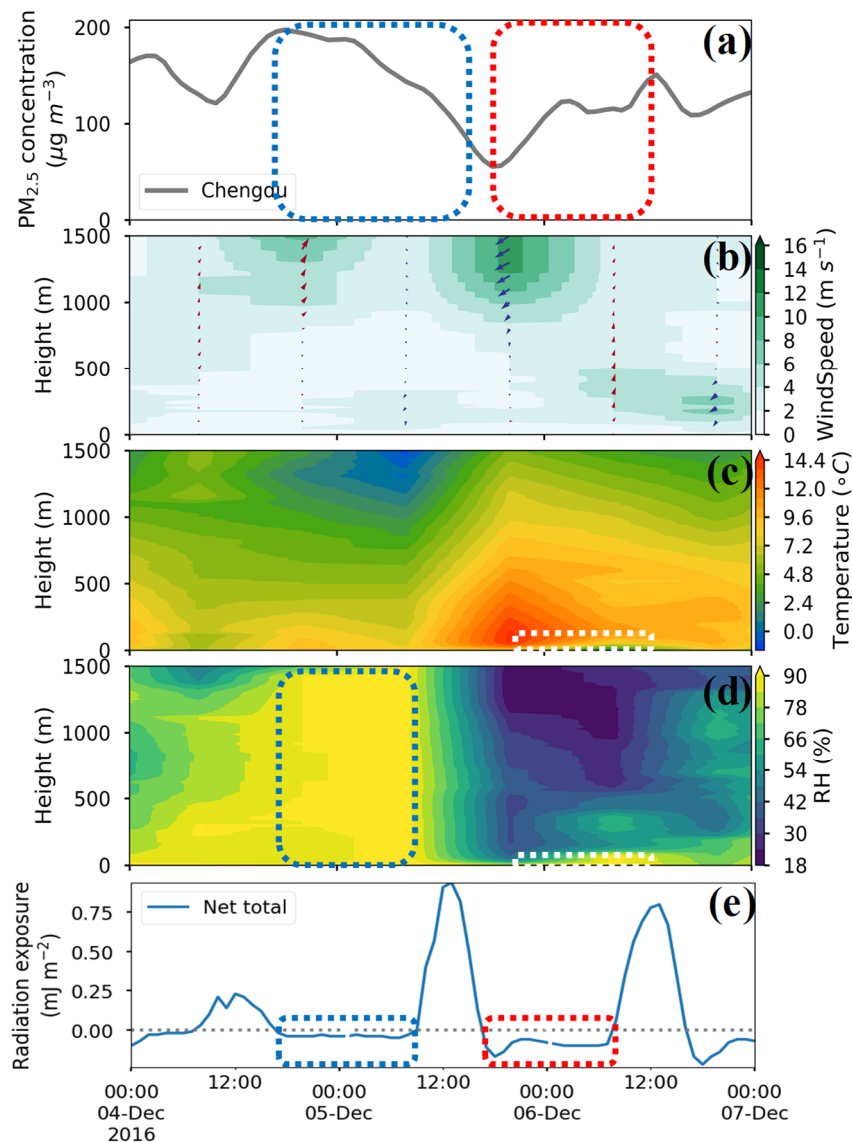
457 From December 1, 2016, to January 10, 2017, three HPEs appeared in Chengdu (Fig. 12, blue boxes),
 458 and these episodes lasted for more than 10 days and had peak mass concentrations greater than 200 μg
 459 m⁻³ (Fig. 12 (a)). During these three episodes, we observed thick mid-upper level fog/clouds above
 460 Chengdu (Fig. 12 (d)), which was blocked by the surrounding mountains and upper-level inversions. The
 461 mid-upper level cloud competes with the near-surface aerosols for solar radiation, i.e., as more solar
 462 radiation is reflected by the mid-upper layer cloud, the near-surface aerosols receive less solar radiation.

463 Therefore, with cloudy mid-upper layers, more solar radiation is reflected to cool the atmosphere below
 464 the clouds, and this condition suppresses the two-way feedback mechanism between the unfavorable
 465 weather conditions and the near-surface aerosols. Consequently, the two-way feedback was weak and
 466 nearly no near-ground temperature inversion was observed (Fig. 12 (c)). Despite the lack of a two-way
 467 feedback mechanism to aggravate aerosol pollution, the increase in the PM_{2.5} mass concentration is still
 468 under stable stratification dominated by slight or calm winds (Fig. 12, red boxes). Comparing the RH
 469 variations in the two process of increasing PM_{2.5} (Fig. 12 red boxes) during the HPE from December 26,
 470 2016, to January 6, 2017, we found that the PM_{2.5} mass concentration increases correspondingly with the
 471 lower RH.



472
 473 **Figure 13: Vertical section of mean air temperature in December 2016 at 30.67°N.**

474 In addition to the near-surface weak winds, persistent aerosol pollution is a result of temperature
 475 inversions caused by the warm southwest advection (Fig. 12 (b, c), brown boxes). The ground of the
 476 Qinghai-Tibet Plateau is a heat source throughout the year (Ye and Gao, 1979); thus, it heats the near-
 477 surface ambient air (Fig. 13). When the relatively warm air moves east across the Tibet Plateau under the
 478 southwesterly winds, it forms an inversion above the basin (Fig. 12 (c), brown boxes), which caps the
 479 convective layer and then induces the accumulation of aerosols and water vapor.



480

481 **Figure 14: Temporal variations in PM_{2.5}, surface radiation and vertical distributions of meteorological**
 482 **factors from December 4 to 7, 2017. (a) PM_{2.5} mass concentration (gray line: Chengdu); (b) winds (vectors) and**
 483 **wind velocity (shadings; units: m s⁻¹); (c) temperature (shadings; units: °C); (d) RH (shadings; units: %); and (e)**
 484 **global radiant exposure.**

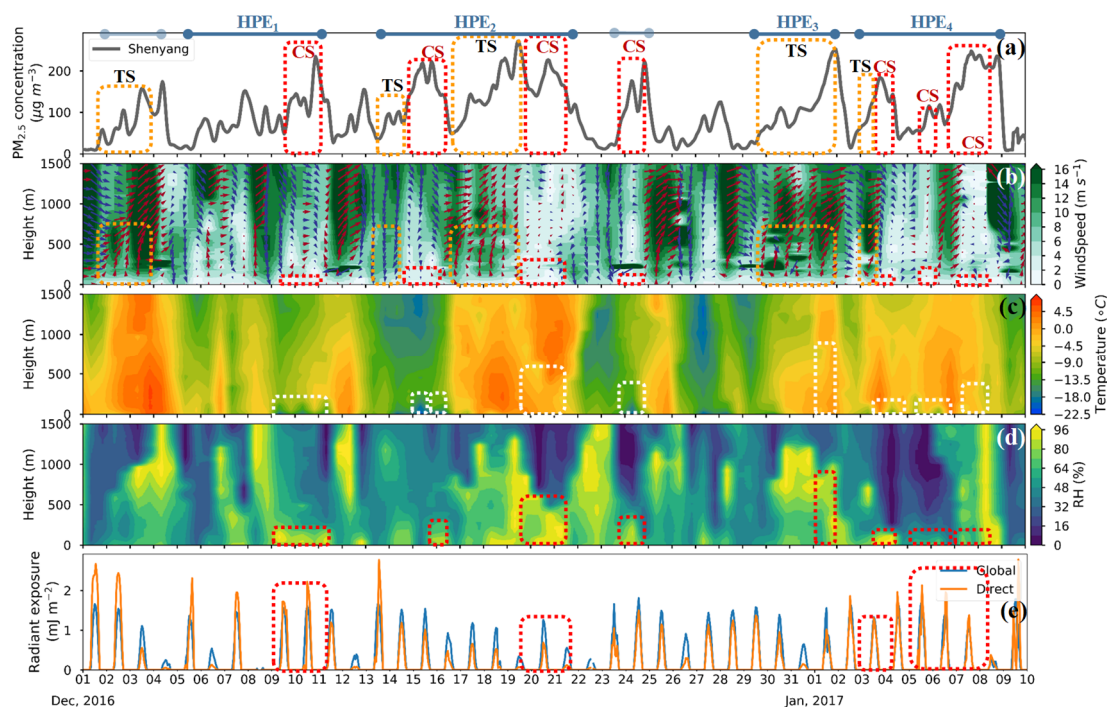
485 Effective pollution clearing rarely occurs in Chengdu because the Sichuan Basin is less affected by
 486 the cold, clean northerly winds as a result of the surrounding high northern mountains. However, as soon
 487 as aerosol pollutants and water vapor are cleared, aerosol pollution will form again due to more longwave
 488 radiation lost from the ground. For example, during December 4-7, 2016, the fog/cloud dissipated, and
 489 the PM_{2.5} mass concentration dropped to a low value on the 5th (Fig. 14 (a, d)). Due to the absence of
 490 cloud/fog blocking, more longwave radiation from the ground was emitted into space on the 6th night,
 491 and the surface net radiant exposure decreased from -0.58 on the 5th to -1.45 on the 6th (2.5 times) (Fig.

492 14 (e)). The significant reduction in the surface radiation cooled the near-surface atmospheric
 493 temperature, which formed an inversion layer of approximately 50~100 m (Fig. 14 (c)). Capped by the
 494 inversion layer, the PM_{2.5} mass concentration doubled after the night of the 6th to form another aerosol
 495 pollution event ((Fig. 14 (a)).

496 Pollution removal in Chengdu mainly relies on northeasterly winds to blow pollution away. The
 497 winds also carry water vapor to add humidity to the atmosphere above Chengdu, which converts
 498 pollutants into fog/cloud drops or produces precipitation that removes pollutants through wet removal
 499 (Fig. 12 (d), blue boxes).

500 **3.6 The two-way feedback mechanism on the windy Northeast China Plain, where mid-lower**
 501 **warm, humid southwesterly winds transport aerosol pollutants from polluted southwestern**
 502 **regions, and strong, clean northwesterly winds blow pollutants away.**

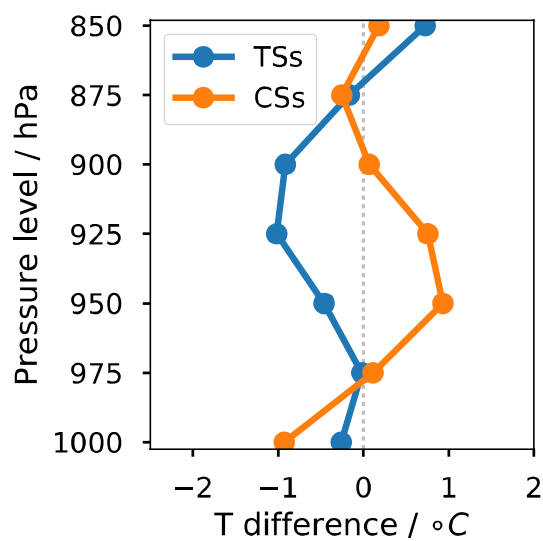
503 The Northeast China Plain lies north of the Liaodong Gulf, west of the Changbai Mountains, east
 504 of the Greater Khingan, and south of the Lesser Khingan (Fig. 2). Due to the low mountains to the
 505 northwest, the Northeast China Plain is susceptible to cold, dry northerly air from Siberia in winter. As
 506 the largest city in Northeast China regarding its urban population, Shenyang is located in the
 507 southwestern Northeast China Plain (Fig. 2), where the warm, humid southwesterly flows are transported
 508 from Bohai Bay.



509 **Figure 15: Temporal variations in PM_{2.5}, surface radiation and vertical distributions of meteorological**
 510 **factors from December 1, 2016, to January 10, 2017. (a) PM_{2.5} mass concentration (gray line: Shenyang); (b)**
 511

512 winds (vectors) and wind velocity (shadings; units: m s^{-1}); (c) temperature (shadings; units: $^{\circ}\text{C}$); (d) RH (shadings;
 513 units: %); and (e) global radiant exposure. (Blue line: HPEs; light blue line: PEs; white or red box: CSs; and blue
 514 dot: precipitation)

515 From December 1, 2016, to January 10, 2017, six aerosol pollution episodes appeared in Shenyang
 516 (Fig. 15 (a), blue boxes), four of which persisted for more than 3 days with peak $\text{PM}_{2.5}$ mass
 517 concentrations greater than $200 \mu\text{g m}^{-3}$ (Fig. 15 (a)). During these HPEs, we observed surface radiation
 518 reductions, near-surface inversions, low-level RH enhancement, and increases in the $\text{PM}_{2.5}$ mass
 519 concentration (Fig. 15 (a, c, d), red and white boxes) under slight or calm winds (Fig. 15 (b), red boxes);
 520 these conditions indicate the occurrence of the two-way feedback mechanism in Shenyang.



521
 522 **Figure 16: Vertical mean temperature difference between sounding observations and ERA-interim**
 523 **reanalysis data during TSs and CSs in Shenyang from December 1, 2016, to January 10, 2017.**

524 To quantify the magnitude of the two-way feedback during TSs and CSs in Shenyang, the air
 525 temperature difference between the radiosonde observations at 2000 BJT and the ERA-interim reanalysis
 526 data was obtained. Similar to Beijing and Xi'an, the temperature profile was also modified by aerosols
 527 during both the TSs and the CSs (Fig.16 (a, b)). However, the magnitude of near-ground cooling bias
 528 was lower than that in Beijing and Xi'an, which is due to relatively light aerosol pollution and windy
 529 conditions. From TSs to CSs, the negative temperature difference at 1000 hPa increased from $-0.26 \text{ }^{\circ}\text{C}$
 530 to $-0.93 \text{ }^{\circ}\text{C}$. The mean aerosol-induced cooling bias (1000 hPa) in the TSs was only 28.2% of that in the
 531 CSs.

532 Compared with those in Xi'an, Nanjing, Wuhan, Qingyuan, and Chengdu, the speeds of the
 533 southeasterly or northwesterly winds are strikingly higher in Shenyang. Relatively strong mid-lower
 534 southeasterly winds originate from Bohai Bay, and these winds transport warm, humid air that heats and

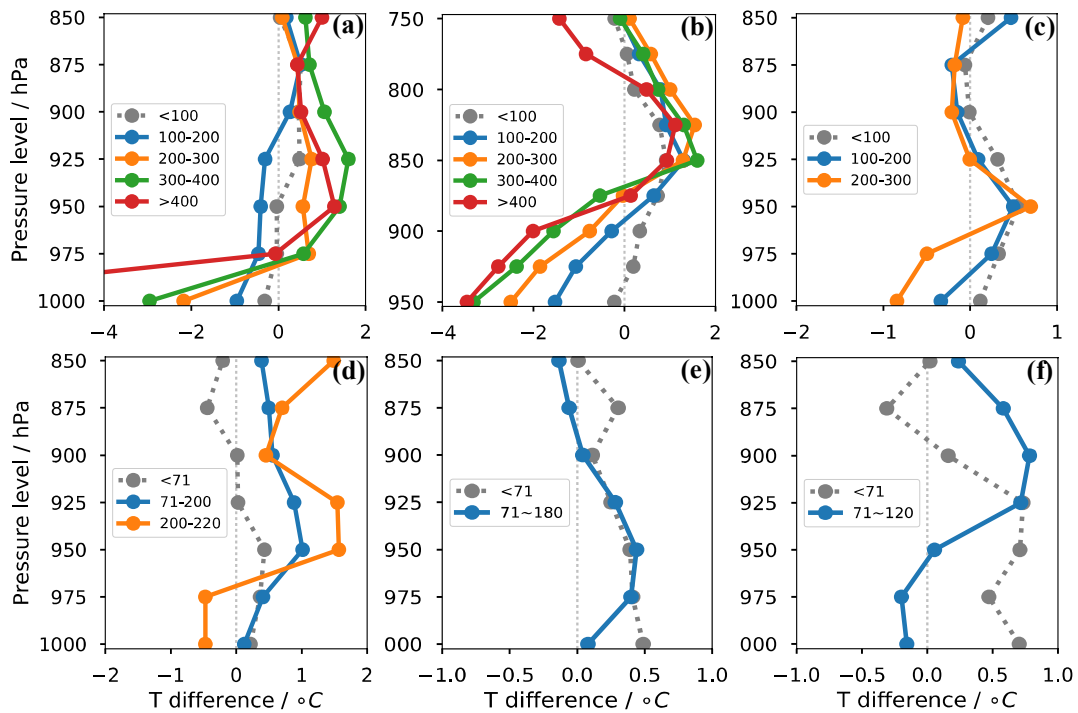
535 adds humidity to the mid-upper layer above Shenyang (Fig. 15 (c, d)). This air also transports aerosol
536 pollutants to Shenyang because it carries pollutants from populated and polluted southwestern industrial
537 regions, including Anshan. Lower strong northwesterly winds carry dry, cold air from Siberia to remove
538 pollutants in Shenyang (Fig. 15 (a, b)).

539 **3.7 Quantifying the two-way feedback mechanism and comparing its magnitude in various haze** 540 **regions of China.**

541 As previously mentioned, the weak two-way feedback mechanism in the Sichuan Basin is weakened
542 by the cloudy mid-upper layers, which compete with the near-surface aerosols for solar radiation.
543 However, the mechanism occurred in the Guanzhong Plain, the middle and lower reaches of the Yangtze
544 River, the Pearl River Delta region, and the Northeast China Plain. Dominant scattering aerosols will
545 scatter solar radiation to cause near-ground temperature reduction; Absorbing aerosols will absorb solar
546 radiation to heat the upper aerosol layer and subsequently cool the near-ground layer (Boucher et al.,
547 2013a). Previous studies found that aerosol profiles play an important part in radiative cooling effects of
548 aerosols, which results in vertical differences in meteorological factors (Wilcox et al., 2016; Wang et al.,
549 2018). To quantify the magnitude of the two-way feedback in these haze regions of China, we obtained
550 the vertical air temperature difference between the radiosonde observations affected by this two-way
551 feedback and the ERA-interim reanalysis data without feedback in the regional center cities, including
552 Beijing, Xi'an, Shenyang, Wuhan, Nanjing, and Qingyuan (to replace Guangzhou). A previous study
553 established a threshold value for the PM_{2.5} mass concentration ($100 \mu\text{g m}^{-3}$) that effectively activates the
554 two-way feedback in HPEs; additionally, a lower threshold value ($71 \mu\text{g m}^{-3}$) has been identified for
555 lighter HPEs (Zhong et al., 2019). Therefore, based on the diurnal mean PM_{2.5} mass concentration (from
556 08:00 to 17:00 BJT), the temperature difference is further classified by the criterion of $100 \mu\text{g m}^{-3}$ in the
557 more polluted North China Plain, Guanzhong Plain, and Northeast China Plain and by the criterion of 71
558 $\mu\text{g m}^{-3}$ in the less polluted Two Lakes Plain, Yangtze River Delta, and Pearl River Delta.

559 By comparing the air temperature difference below and above these thresholds in the six cities, we
560 found that the lower temperature profile was strikingly modified by the two-way feedback mechanism
561 (Fig. 17). On the North China Plain, the Guanzhong Plain, and the Northeast China Plain, the lower
562 temperature bias between the sounding observations and the ERA-interim data was close to zero below
563 the threshold of $100 \mu\text{g m}^{-3}$ but immediately became negative above the threshold (Fig. 17 (a, b, c)). In

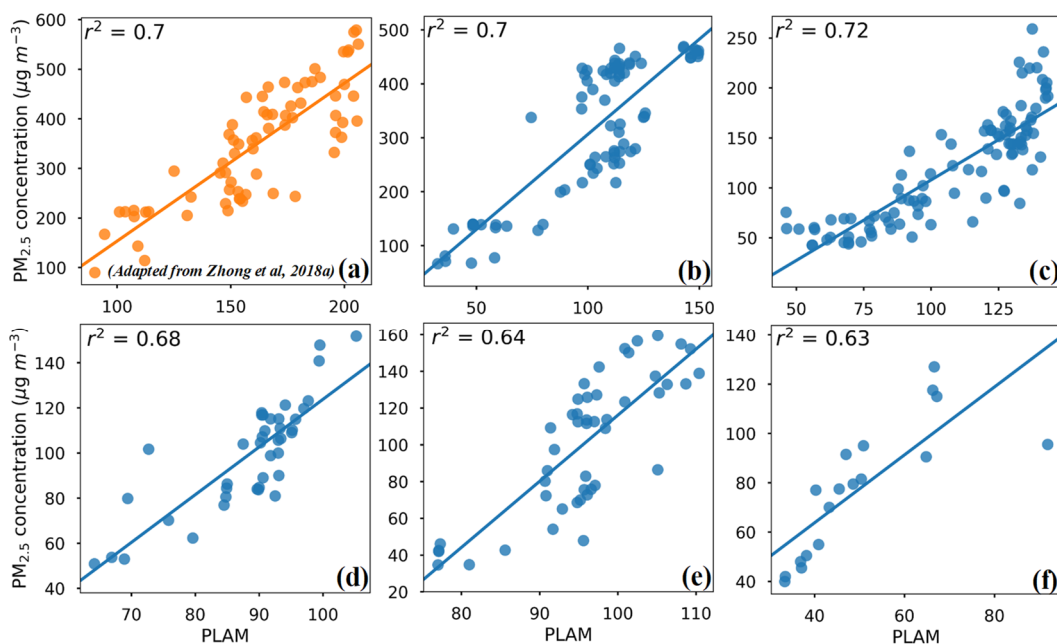
564 the Two Lakes Plain, the Yangtze River Delta, and the Pearl River Delta, we observed a similar reduction
 565 in the temperature difference below and above the threshold of $71 \mu\text{g m}^{-3}$ (Fig. 17 (d, e, f)). Overall, the
 566 magnitude of the two-way feedback mechanism was larger in the North China Plain, the Guanzhong
 567 Plain, and the Northeast China Plain than in the Two Lakes Plain, the Yangtze River Delta, and the Pearl
 568 River Delta.



569
 570 **Figure 17: Vertical temperature difference between sounding observations and ERA-interim reanalysis data**
 571 **under different concentration bins of $\text{PM}_{2.5}$ mass ($\mu\text{g m}^{-3}$).** (a) Beijing; (b) Xi'an; (c) Shenyang; (d) Wuhan; (e)
 572 Nanjing; and (f) Qingyuan.

573 For each representative site, the low-level cooling bias was more striking near the ground surface;
 574 additionally, as the $\text{PM}_{2.5}$ mass concentration increased, the low-level cooling bias became more
 575 significant (Fig. 17). In Beijing, the negative temperature difference reached more than 2°C with $\text{PM}_{2.5}$
 576 values in the range of $200 \sim 300 \mu\text{g m}^{-3}$ compared to approximately 1°C in the range of $100 \sim 200 \mu\text{g m}$
 577 $^{-3}$. In Xi'an, the temperature difference decreased from approximately -1.5°C in the range of $100 \sim 200$
 578 $\mu\text{g m}^{-3}$ to 2.5°C in the range of $200 \sim 300 \mu\text{g m}^{-3}$. In Shenyang, the cooling bias of approximately 0.6°C
 579 occurred with the increase in $\text{PM}_{2.5}$ from $100 \sim 200 \mu\text{g m}^{-3}$ to $200 \sim 300 \mu\text{g m}^{-3}$. Under the most polluted
 580 conditions, the near-ground cooling bias was greater than -4°C , approximately -4°C , and approximately
 581 -1°C in Beijing, Xi'an, and Shenyang, respectively, which was substantially affected by the two-way
 582 feedback.

583 To quantify the feedback of the worsened meteorological conditions on the increasing PM_{2.5} in the
 584 CSs, a PLAM index was used, which mainly reflects the stability of the air mass and the condensation
 585 rate of water vapor on aerosol particles. The squared correlation coefficients between the hourly PLAM
 586 and PM_{2.5} mass concentration in the typical PM_{2.5} increase processes during the CSs were 0.71, 0.7, 0.72,
 587 0.68, 0.64, and 0.63 in Beijing, Xi'an, Shenyang, Wuhan, Nanjing, and Qingyuan, respectively (Fig. 18
 588 (a, b, c, d, e, f)); these values exceeded the 0.05 significance level, which suggested that such a
 589 meteorological feedback on PM_{2.5} explained 60~70% of the increase in the PM_{2.5} during the CSs.



590
 591 **Figure 18: Correlation between PLAM and PM_{2.5} during the typical rising processes of PM_{2.5} from**
 592 **December 1, 2016 to January 10, 2017.**

593 **4 Conclusions:**

594 Here, we used PM_{2.5} observations, surface radiation data, radiosonde observations, meteorological
 595 index-PLAM, and ERA-interim reanalysis data to investigate the formation, accumulation, and
 596 dispersion of aerosol pollution during persistent heavy aerosol pollution episodes over 3 days (HPEs),
 597 particularly focusing on the two-way feedback mechanism between the unfavorable meteorological
 598 conditions and the cumulative PM_{2.5} pollution in various haze regions in China, including the Guanzhong
 599 Plain, the Yangtze River Delta region, the Two Lakes Basin, the Pearl River Delta, the Sichuan Basin,
 600 and the Northeast China Plain.

601 On the Guanzhong Plain, we observed a striking two-way feedback mechanism, including reduced

602 surface radiations, near-surface inversions, RH enhancement in the lower part of BL, and increases in
603 PM_{2.5} mass concentrations under slight or calm winds in the CSs. For the representative sites of Xi'an,
604 the near-ground cooling bias caused by the two-way feedback was as high as approximately -4 °C, which
605 was similar to that observed in Beijing. Bordered by the Qinling Mountains and the Loess Plateau, the
606 Guanzhong Plain experiences inter-regional pollution transport below the BL, e.g., pollution transport to
607 Xi'an from Yuncheng and Linfen under lower northwesterly winds in the TSs. Pollution clearing mainly
608 depends on the lower strong northeasterly winds to blow pollutants away and the mid-upper southerly
609 winds to transport water vapor to increase RH, which causes the PM_{2.5} to enter the fog-cloud phase.

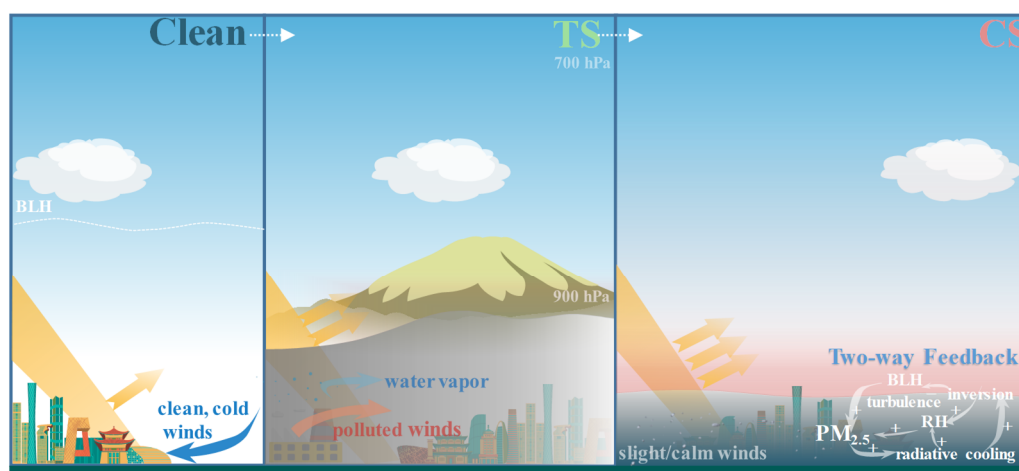
610 In the relative less polluted Yangtze River Delta region, the aerosol pollution formation is similar to
611 that in Beijing, including earlier TSs and later CSs. During the TSs, the Yangtze River Delta region is
612 affected by trans-regional pollution transport below and over the BL from the North China Plain, which
613 induces increases in the PM_{2.5} in near-surface or at the higher atmosphere in this region, which includes
614 Nanjing and Shanghai. Upper transported pollutants would move downward to worsen the near-ground
615 aerosol pollution further. During the CSs, we also observed the two-way feedback mechanism, but its
616 magnitude is lower than that in Beijing due to the less-polluted conditions. In this region, pollution
617 clearing relies on persistent stronger northerly winds bring pollutants out of this area, or strong
618 southeasterly winds, which transport clean, warm, humid air that blows pollutants away or increases
619 ambient RH to cause the PM_{2.5} to enter the liquid fog-cloud phase. Similar to the Yangtze River Delta
620 region, the Two Lakes Basin also experienced trans-regional pollution transport from the North China
621 Plain under northerly winds below and sometimes over the BL during the TSs. During the CSs, the two-
622 way feedback is activated, and the aerosol pollution worsens. In addition to the blowing effect of strong,
623 persistent northerly winds, pollution clearing also depends on the mid-upper southerly winds, particularly
624 the southwesterly winds, to transport water vapor, which enhances the RH and eliminates pollutants
625 through fog-cloud conversion and wet removal.

626 In the least polluted Pearl River Delta, no feedback mechanism was observed with PM_{2.5} mass
627 concentrations below the threshold. However, when the PM_{2.5} concentration exceeded the threshold, the
628 two-way feedback occurred in the CSs. The delta region was purified by lower clean, cold northeasterly
629 winds from the northern mountains and humidified by upper southerly winds from the South China Sea.

630 The Sichuan Basin is dominated by high RH and weak winds; thus, the two-way feedback

631 mechanism was weakened by thick mid-upper fog/clouds that compete with the near-surface aerosols for
 632 solar radiation and consequently cool the whole atmosphere below. With the weak two-way feedback,
 633 the PM_{2.5} mass concentration increased under lower slight or calm winds and was capped by the upper
 634 temperature inversions caused by the upper southwesterly winds from the Tibet Plateau. Pollution
 635 clearing mainly relies on northeasterly winds to blow pollutants away, and these winds also add humid
 636 air to the atmosphere, which converts aerosols into fog/cloud drops. Although pollutants and water vapor
 637 are cleared, aerosol pollution will soon form again due to more longwave radiation lost from the ground,
 638 which results in rare effective pollution clearing in the Sichuan Basin.

639 Compared with the above regions, the southerly and northerly winds are strikingly larger in the
 640 Northeast China Plain. Strong mid-lower southeasterly winds originate from Bohai Bay, transport warm,
 641 humid air that heats and adds humidity to the inland area and transport pollutants inter-regionally from
 642 polluted southwestern industrial regions. Lower strong northwesterly winds carry dry, cold air from
 643 Siberia to remove pollutants. At the representative site in Shenyang, a two-way feedback mechanism also
 644 exists during the CSs with slight or calm winds.



645
 646 **Figure 19: A concept scheme of pollution removal (a), transport (b), and accumulation (c), particularly the**
 647 **two-way feedback mechanism between the unfavorable meteorological conditions and the cumulative**
 648 **aerosol pollution (c).**

649 The transport, accumulation, and removal of pollution described above are visually illustrated in a
 650 conceptual scheme (Fig. 19), which particularly highlights the effect of the two-way feedback mechanism
 651 in the role of intensifying the HPEs. Due to the occurrence of a two-way feedback mechanism, effective
 652 pollution control could further mitigate aerosol pollution, while persistent worsening aerosol pollution

653 could lead to an additional increase in PM_{2.5}. Given the inter-regional and trans-regional pollution
654 transport, the control of regional emissions among key haze regions in China, to reduce the pollutants
655 transport or to let them not reach the threshold enough to trigger two-way feedback mechanism, is
656 essential to reduce persistent heavy aerosol pollution episodes substantially. At the same time, these
657 results also show that, even in favorable weather conditions, aerosol pollutant emissions should not be
658 allowed to occur without restrictions; when aerosol pollution cumulates to a certain extent, it will
659 significantly worsen the BL meteorological conditions and "close" the "meteorological channels"
660 available for pollution dispersion.

661

662 **Acknowledgment:**

663 This research is supported by the National Key Project of MOST (2016YFC0203306) and the
664 Atmospheric Pollution Control of the Prime Minister Fund (DQGG0104).

665 **Author Contributions:**

666 X.Y.Z. and Y.Q.W. designed the research; X.Y.Z and J.T.Z carried out the analysis of observations.
667 T.J.W provided UAV observations. J.Z.W provided PLAM data. X.J.S conducted a supplementary
668 analysis. J.T.Z. wrote the first manuscript and X.Y.Z. revised it. All authors contributed to the
669 improvement of this manuscript and approved the final version.

670 **Additional Information:**

671 Competing financial interests: The authors declare no competing financial interests.

672

673 **References:**

- 674 Bai, N., et al.: The pharmacology of particulate matter air pollution-induced cardiovascular
675 dysfunction, *Pharmacol. Ther.*, 113, 16-29, 2007.
- 676 Boucher, O., et al.: Clouds and aerosols, in: *Climate change 2013: the physical science basis.*
677 *Contribution of Working Group I to the Fifth Assessment Report of the Intergovernmental Panel*
678 *on Climate Change*, Cambridge University Press, 571-657, 2013a.
- 679 Boucher, O., et al.: Clouds and Aerosols, in: *Climate Change 2013: The Physical Science Basis.*
680 *Contribution of Working Group I to the Fifth Assessment Report of the Intergovernmental Panel*
681 *on Climate Change*, edited by: Stocker, T. F., Qin, D., Plattner, G.-K., Tignor, M., Allen, S. K.,
682 Boschung, J., Nauels, A., Xia, Y., Bex, V., and Midgley, P. M., Cambridge University Press, Cambridge,
683 United Kingdom and New York, NY, USA, 571-658, 2013b.
- 684 Chen, Y., et al.: Evidence on the impact of sustained exposure to air pollution on life expectancy
685 from China's Huai River policy, *PNAS*, 110, 12936-12941, 10.1073/pnas.1300018110, 2013.
- 686 Cheng, Y., et al.: Reactive nitrogen chemistry in aerosol water as a source of sulfate during haze
687 events in China, *Sci. Adv.*, 2, e1601530, 10.1126/sciadv.1601530, 2016.
- 688 Dee, D. P., et al.: The ERA-Interim reanalysis: configuration and performance of the data
689 assimilation system, *Q. J. R. Meteorolog. Soc.*, 137, 553-597, doi:10.1002/qj.828, 2011.
- 690 Ding, A. J., et al.: Enhanced haze pollution by black carbon in megacities in China, *Geophys. Res.*
691 *Lett.*, 43, 2016.
- 692 Ervens, B., et al.: Secondary organic aerosol formation in cloud droplets and aqueous particles
693 (aqSOA): a review of laboratory, field and model studies, *Atmos. Chem. Phys.*, 11, 11069-11102,
694 10.5194/acp-11-11069-2011, 2011.
- 695 Fang, S., et al.: Parameterization and comparative evaluation of the CCN number concentration
696 on Mt. Huang, China, *Atmos. Res.*, 181, 300-311, 10.1016/j.atmosres.2016.07.004, 2016.
- 697 Huang, X., et al.: Impact of Aerosol-PBL Interaction on Haze Pollution: Multiyear Observational
698 Evidences in North China, *Geophys. Res. Lett.*, 0, doi:10.1029/2018GL079239, 2018.
- 699 Ji, D., et al.: The heaviest particulate air-pollution episodes occurred in northern China in January,
700 2013: insights gained from observation, *Atmos. Environ.*, 92, 546-556, 2014.
- 701 Kuang, Y., et al.: Impact of aerosol hygroscopic growth on the direct aerosol radiative effect in
702 summer on North China Plain, *Atmospheric Environment*, 147, 224-233, 2016.
- 703 Matus, K., et al.: Health damages from air pollution in China, *Global Environ. Change*, 22, 55-66,
704 2012.
- 705 Pilinis, C., et al.: Water content of atmospheric aerosols, *Atmos. Environ.*, 23, 1601-1606, 1989.
- 706 Poli, P., et al.: Assimilation of Global Positioning System radio occultation data in the ECMWF ERA-
707 Interim reanalysis, *Q. J. R. Meteorolog. Soc.*, 136, 1972-1990, 2010.
- 708 Simmons, A.: ERA-Interim: New ECMWF reanalysis products from 1989 onwards, *ECMWF*
709 *newsletter*, 110, 25-36, 2006.
- 710 Su, F., et al.: Transport pathways of pollutants from outside in atmosphere boundary layer, *Res.*
711 *Environ. Sci.*, 1, 26-29, 2004.
- 712 Tao, S.: *Error Analyses for Temperature of L Band Radiosonde*, Meteorological, 2006.
- 713 Thépaut, J. N., et al.: Dynamical structure functions in a four-dimensional variational assimilation:
714 A case study, *Q. J. R. Meteorolog. Soc.*, 122, 535-561, 1996.
- 715 Tie, X., et al.: Severe Pollution in China Amplified by Atmospheric Moisture, *Sci. Rep.*, 7, 15760,
716 10.1038/s41598-017-15909-1, 2017.

717 Wang, J., et al.: Diagnostic identification of the impact of meteorological conditions on PM2.5
718 concentrations in Beijing, *Atmos. Environ.*, 81, 158-165, 10.1016/j.atmosenv.2013.08.033, 2013.

719 Wang, J. Z., et al.: A parameterized method for air-quality diagnosis and its applications, *Advance*
720 *of Meteorology*, doi:10.1155/2012/238589, 1-10, 2012.

721 Wang, Z., et al.: Dome effect of black carbon and its key influencing factors: a one-dimensional
722 modelling study, *Atmos. Chem. Phys.*, 18, 2821-2834, 10.5194/acp-18-2821-2018, 2018.

723 Wilcox, E. M., et al.: Black carbon solar absorption suppresses turbulence in the atmospheric
724 boundary layer, *Proceedings of the National Academy of Sciences*, 113, 11794-11799, 2016.

725 Yang, Q., et al.: Spatial distribution pattern of population and characteristics of its evolution in
726 China during 1935-2010, *Geographical Research*, 35, 1547-1560, 2016.

727 Ye, D., and Gao, Y.: *Meteorology of the Tibetan Plateau*, Science Publication Agency, Beijing (in
728 Chinese). Google Scholar, 1979.

729 Zhang, Q., et al.: Asian emissions in 2006 for the NASA INTEX-B mission, *Atmos. Chem. Phys.*, 9,
730 5131-5153, 2009a.

731 Zhang, Q., et al.: Cleaning China's air, *Nature*, 484, 161, 10.1038/484161a, 2012a.

732 Zhang, X., et al.: Factors contributing to haze and fog in China, *Chin. Sci. Bull.*, 58, 1178,
733 10.1360/972013-150, 2013.

734 Zhang, X. Y., et al.: Changes of Atmospheric Composition and Optical Properties Over BEIJING—
735 2008 Olympic Monitoring Campaign, *Bull. Am. Meteorol. Soc.*, 90, 1633-1651, 2009b.

736 Zhang, X. Y., et al.: Atmospheric aerosol compositions in China: spatial/temporal variability,
737 chemical signature, regional haze distribution and comparisons with global aerosols, *Atmos. Chem.*
738 *Phys.*, 12, 779-799, 10.5194/acp-12-779-2012, 2012b.

739 Zhang, X. Y., et al.: Changes in chemical components of aerosol particles in different haze regions
740 in China from 2006 to 2013 and contribution of meteorological factors, *Atmos. Chem. Phys.*, 15,
741 12935-12952, 10.5194/acp-15-12935-2015, 2015.

742 Zhong, J., et al.: Relative contributions of boundary-layer meteorological factors to the explosive
743 growth of PM 2.5 during the red-alert heavy pollution episodes in Beijing in December 2016, *J.*
744 *Meteorolog. Res.*, 31, 809-819, 2017.

745 Zhong, J., et al.: Feedback effects of boundary-layer meteorological factors on cumulative
746 explosive growth of PM2.5 during winter heavy pollution episodes in Beijing from 2013 to 2016,
747 *Atmos. Chem. Phys.*, 18, 247-258, 10.5194/acp-18-247-2018, 2018a.

748 Zhong, J., et al.: Heavy aerosol pollution episodes in winter Beijing enhanced by radiative cooling
749 effects of aerosols, *Atmos. Res.*, 209, 59-64, <https://doi.org/10.1016/j.atmosres.2018.03.011>,
750 2018b.

751 Zhong, J., et al.: Reflections on the threshold for PM2.5 explosive growth in the cumulative stage
752 of winter heavy aerosol pollution episodes (HPEs) in Beijing, *Tellus B: Chemical and Physical*
753 *Meteorology*, 71, 1-7, 10.1080/16000889.2018.1528134, 2019.

754 Zhou, S., et al.: The Characteristics and Contributing Factors of Air Pollution in Nanjing: A Case
755 Study Based on an Unmanned Aerial Vehicle Experiment and Multiple Datasets, *Atmosphere*, 9,
756 343, 10.3390/atmos9090343, 2018.

757 Zhu, W., et al.: The characteristics of abnormal wintertime pollution events in the Jing-Jin-Ji region
758 and its relationships with meteorological factors, *Sci. Total Environ.*, 626, 887, 2018.

759